

Ground states and dynamics of multi-component Bose-Einstein condensates

Weizhu Bao *

Department of Computational Science
National University of Singapore, Singapore 117543

Abstract

We study numerically the time-independent vector Gross-Pitaevskii equations (VGPEs) for ground states and time-dependent VGPEs with (or without) an external driven field for dynamics describing a multi-component Bose-Einstein condensate (BEC) at zero or very low temperature. In preparation for the numerics, we scale the 3d VGPEs, approximately reduce it to lower dimensions, present a normalized gradient flow (NGF) to compute ground states of multi-component BEC, prove energy diminishing of the NGF which provides a mathematical justification, discretize it by the backward Euler finite difference (BEFD) which is monotone in linear and nonlinear cases and preserves energy diminishing property in linear case. Then we use a time-splitting sine-spectral method (TSSP) to discretize the time-dependent VGPEs with an external driven field for computing dynamics of multi-component BEC. The merit of the TSSP for VGPEs is that it is explicit, unconditionally stable, time reversible and time transverse invariant if the VGPEs is, ‘good’ resolution in the semiclassical regime, of spectral order accuracy in space and second order accuracy in time, and conserves the total particle number in the discretized level. Extensive numerical examples in 3d for ground states and dynamics of multi-component BEC are presented to demonstrate the power of the numerical methods and to discuss the physics of multi-component Bose-Einstein condensates.

Key Words. Multi-component, Bose-Einstein condensate (BEC), Vector Gross-Pitaevskii equations (VGPEs), Normalized gradient flow, Monotone scheme, Energy diminishing, Ground states, Time-splitting sine spectral (TSSP) method.

*Email address: bao@cz3.nus.edu.sg.

1 Introduction

Since its realization in dilute atomic gases [2, 12], Bose-Einstein condensation (BEC) of alkali atoms and hydrogen has been produced and studied extensively in the laboratory [27], and has afforded an intriguing glimpse into the macroscopic quantum world. In view of potential applications, such as the generation of bright beams of coherent matter waves (atom laser), a central goal has been the formation of condensate with the number of atoms as large as possible. It is thus of particular interest to study a scenario where this goal is achieved by uniting two (or more) independently grown condensates to form one large single condensate. The first experiment involving the uniting of multiple-component BEC was performed with atoms evaporatively cooled in the $|F = 2, m_f = 2\rangle$ and $|1, -1\rangle$ spin states of ^{87}Rb [39]. Physically speaking, two independently formed condensates are characterized by a random relative phase of their macroscopic wave functions. A “fusing” of two condensates thus amounts to locking the relative phase in a dissipative process. Currently, there are two typical ways to lock the relative phase: (i). An external driven field [39]; (ii). An internal atomic Josephson junction [30]. In fact, recent experimental advances in exploration of systems of uniting two or more condensates, e.g. in a magnetic trap in rubidium [39] and subsequently in an optical trap in Sodium [45], have spurred great excitement in the atomic physics community and renewed interest in studying the ground states and dynamics of multi-component BEC [27, 18, 30, 20].

Theoretical treatment of such systems began in the context of superfluid helium mixtures [32] and spinpolarized hydrogen [44], and has now been extended to BEC in the alkalis [28, 23, 35, 41]. Theoretical predications of properties of uniting two or more condensates, e.g. density profile, dynamics of interacting BEC condensates [24], motional damping [30] and formation of vortices [31, 33, 36], can now be compared with experimental data [27, 3]. Needless to say that this dramatic progress on the experimental front has stimulated a wave of activity on both the theoretical and the numerical front. In fact, the properties of uniting two or more BEC states at temperatures T much smaller than the critical condensation temperature T_c [34] are usually modeled by the vector Gross-Pitaevskii equations (VGPSs) for the macroscopic vector wave function [40, 34] either with an external driven field [27] or with an internal atomic Josephson junction [30]. Note that equations very similar to the VGPEs also appear in nonlinear optics where indices of refraction, which depend on the light intensity, leads to nonlinear terms like those encountered in VGPEs.

There have been extensive numerical studies of the time-independent Gross-Pitaevskii equation (GPE) for ground states and time-dependent GPE for dynamics of single-component BEC. For computing ground states of BEC, Bao and Du [4] presented a normalized gradient flow (NGF), proved energy diminishing and discretized it by a backward Euler finite difference (BEFD) method; Bao and Tang [11] proposed a method which can be used to compute the ground and excited states via directly minimizing the energy functional; Edwards and Burnett [22] introduced a Runge-Kutta type method; other methods include an explicit imaginary-time al-

gorithm used in [1] and [19]; a directly inversion in the iterated subspace (DIIS) used in Schneider et al. [43] and a simple analytical type method proposed by Dodd [21]. For numerical solutions of time-dependent GPE for finding dynamics of BEC, Bao et al. [6] presented a time-splitting spectral (TSSP) method, Ruprecht et al. [42] used the Crank-Nicolson finite difference method, Cerimele et al. [16, 17] proposed a particle-inspired scheme. Up to now, only a few numerical simulations on multi-component BEC [30, 18, 25].

In this paper, we take the 3d vector Gross-Pitaevskii equations (VGPEs) with an external driven field for multi-component BEC, make it dimensionless, approximately reduce it to a 2d VGPEs and a 1d VGPEs in certain limits, and discuss the approximate ground state solution of VGPEs in (very) weak interaction regime. Then we present a normalized gradient flow (NGF) to compute ground states of multi-component BEC, prove energy diminishing of the NGF which provides a mathematical justification, discretize it by the backward Euler finite difference (BEFD) which is monotone in linear and nonlinear cases and preserves energy diminishing property in linear case. At last, we use a time-splitting sine-spectral method (TSSP), which was studied in Bao et al. [7, 8] for the nonlinear Schrödinger equation (NLS) in the semiclassical regime and used for GPE of single-component BEC [6], damped GPE for collapse and explosion of BEC [5] and Zakharov system for plasma physics [9, 10], to discretize the time-dependent VGPEs with an external driven field for computing dynamics of multi-component BEC. The merit of the TSSP for VGPEs is that it is explicit, unconditionally stable, easy to program, less memory requirement, time reversible and time transverse invariant if the VGPEs is, ‘good’ resolution in the semiclassical regime, of spectral order accuracy in space and second order accuracy in time, and conserves the total particle number in the discretized level. Extensive numerical examples in 3d for ground states and dynamics of multi-component BEC are presented to demonstrate the power of the numerical methods.

The paper is organized as follows. In section 2 we start out with the 3d VGPEs with an external driven field, make it dimensionless, show how to reduce it to lower dimensions. In section 3 we give approximate ground state solution in (very) weak interaction regime, present a normalized gradient flow (NGF) to compute ground states of multi-component BEC, prove energy diminishing of the NGF, discretize it by the backward Euler finite difference (BEFD), as well as apply the NGF and its BEFD discretization to a nonlinear two-state model for vortex states dynamics in BEC. In section 4, we present the time-splitting sine-spectral (TSSP) method for the VGPEs with an external driven field. In section 5 numerical tests of the VGPEs for ground states and dynamics of multi-component BEC are presented. In section 6 a summary is given. Throughout we adopt the standard l^2 -norm of vectors, matrices, and $\|\cdot\|$ as the standard L^2 -norm for functions, as well as the \ast operator which is used in Matlab for two vectors $\mathbf{U} = (u_1, \dots, u_M)^T$ and $\mathbf{V} = (v_1, \dots, v_M)^T$ as $\mathbf{U} \ast \mathbf{V} = (u_1v_1, \dots, u_Mv_M)^T$.

2 The vector Gross-Pitaevskii equations (VGPEs)

At temperatures T much smaller than the critical temperature T_c [34], a BEC for M components with an external driven field is well described by the macroscopic vector wave function $\Psi = \Psi(\mathbf{x}, t) = (\psi_1(\mathbf{x}, t), \dots, \psi_M(\mathbf{x}, t))^T$ whose evolution is governed by a self-consistent, mean field vector Gross-Pitaevskii equations [26, 40]. If the harmonic trap potential is considered, the VGPEs become

$$i\hbar \frac{\partial \Psi(\mathbf{x}, t)}{\partial t} = -\frac{\hbar^2}{2m} \nabla^2 \Psi(\mathbf{x}, t) + \hat{\mathbf{V}}(\mathbf{x}) * \Psi(\mathbf{x}, t) + \hat{\mathbf{A}}(\Psi) * \Psi(\mathbf{x}, t) + \hbar \hat{f}(t) \hat{B} \Psi(\mathbf{x}, t), \quad (2.1)$$

where $\mathbf{x} = (x, y, z)^T$ is the spatial coordinate vector, m is the atomic mass, $\hbar = 1.05 \times 10^{-34} [J s]$ is the Planck constant, $\hat{f}(t)$ is a given real-valued scalar function, $\hat{B} = (b_{jl})_{j,l=1}^M$ is a given $M \times M$ symmetric real matrix, i.e. $b_{jl} = b_{lj}$ ($j, l = 1, \dots, M$), $\hat{\mathbf{V}}(\mathbf{x}) = (\hat{V}_1(\mathbf{x}), \dots, \hat{V}_M(\mathbf{x}))^T$ is the harmonic trap potential, i.e.

$$\hat{V}_j(\mathbf{x}) = \frac{m}{2} \left(\omega_{x,j}^2 (x - \hat{x}_{0,j})^2 + \omega_{y,j}^2 (y - \hat{y}_{0,j})^2 + \omega_{z,j}^2 (z - \hat{z}_{0,j})^2 \right), \quad j = 1, \dots, M$$

with $(\hat{x}_{0,j}, \hat{y}_{0,j}, \hat{z}_{0,j})^T$ and $\omega_{x,j}, \omega_{y,j}, \omega_{z,j}$ the center and trap frequencies in x , y , and z -direction, respectively, of the j th ($j = 1, \dots, M$) component. For the following we assume (w.r.o.g.) $\omega_{x,1} \leq \dots \leq \omega_{x,M} \leq \omega_{y,1} \leq \dots \leq \omega_{y,M} \leq \omega_{z,1} \leq \dots \leq \omega_{z,M}$. $\hat{\mathbf{A}}(\Psi) = (\hat{A}_1(\Psi), \dots, \hat{A}_M(\Psi))^T$ models the interaction, i.e.

$$\begin{aligned} \hat{A}_j(\Psi) &= u_{j1} |\psi_1|^2 + \dots + u_{jM} |\psi_M|^2 \\ &= \frac{4\pi\hbar^2 a_{j1}}{m} |\psi_1|^2 + \dots + \frac{4\pi\hbar^2 a_{jM}}{m} |\psi_M|^2, \quad j = 1, \dots, M, \end{aligned}$$

with $u_{jl} = \frac{4\pi\hbar^2 a_{jl}}{m}$ and $a_{jl} = a_{lj}$ the s -wave scattering length between the j th and l th component (positive for repulsive interaction and negative for attractive interaction, $j, l = 1, \dots, M$). It is necessary to ensure that the vector wave function is properly normalized. Specifically, we require

$$\int_{\mathbb{R}^3} |\psi_j(\mathbf{x}, 0)|^2 d\mathbf{x} = N_j^0 > 0, \quad j = 1, \dots, M, \quad (2.2)$$

where N_j^0 is the number of particles of the j th ($j = 1 \dots, M$) component at time $t = 0$.

2.1 Dimensionless VGPEs

In order to scale the VGPEs (2.1), we introduce

$$\tilde{t} = \omega_{x,1} t, \quad \tilde{\mathbf{x}} = \frac{\mathbf{x}}{a_0}, \quad \tilde{\psi}_j(\tilde{\mathbf{x}}, \tilde{t}) = \frac{a_0^{3/2}}{\sqrt{N_j^0}} \psi_j(\mathbf{x}, t), \quad j = 1, \dots, M, \quad a_0 = \sqrt{\frac{\hbar}{m\omega_{x,1}}}, \quad (2.3)$$

where a_0 is the length of the harmonic oscillator ground state. In fact, here we choose $1/\omega_{x,1}$ and a_0 as the dimensionless time and length units, respectively. Plugging (2.3) into (2.1), multiplying by $\frac{1}{m\omega_{x,1}^2(N_j^0 a_0)^{1/2}}$ to the j th ($j = 1 \cdots, M$) equation, and then removing all \sim , we obtain the following dimensionless VGPEs in 3d with an external driven field

$$i \frac{\partial \Psi(\mathbf{x}, t)}{\partial t} = -\frac{1}{2} \nabla^2 \Psi(\mathbf{x}, t) + \mathbf{V}(\mathbf{x}) \cdot \Psi(\mathbf{x}, t) + \mathbf{A}(\Psi) \cdot \Psi(\mathbf{x}, t) + f(t) B \Psi(\mathbf{x}, t), \quad (2.4)$$

where $f(t) = \hat{f}(t/\omega_{x,1})/\omega_{x,1}$, and

$$\begin{aligned} \mathbf{V}(\mathbf{x}) &= (V_1(\mathbf{x}), \dots, V_M(\mathbf{x}))^T, \\ V_j(\mathbf{x}) &= \frac{1}{2} \left(\gamma_{x,j}^2 (x - x_{0,j})^2 + \gamma_{y,j}^2 (y - y_{0,j})^2 + \gamma_{z,j}^2 (z - z_{0,j})^2 \right), \\ \gamma_{x,j} &= \frac{\omega_{x,j}}{\omega_{x,1}}, \quad \gamma_{y,j} = \frac{\omega_{y,j}}{\omega_{x,1}}, \quad \gamma_{z,j} = \frac{\omega_{z,j}}{\omega_{x,1}}, \\ x_{0,j} &= \frac{\hat{x}_{0,j}}{a_0}, \quad y_{0,j} = \frac{\hat{y}_{0,j}}{a_0}, \quad z_{0,j} = \frac{\hat{z}_{0,j}}{a_0}, \quad j = 1, \dots, M, \\ \mathbf{A}(\Psi) &= (A_1(\Psi), \dots, A_M(\Psi))^T, \\ A_j(\Psi) &= \beta_{j1} |\psi_1|^2 + \dots + \beta_{jM} |\psi_M|^2, \quad j = 1, \dots, M, \\ \beta_{jl} &= \frac{u_{jl} N_l^0}{a_0^3 \hbar \omega_{x,1}} = \frac{4\pi \hbar^2 a_{jl} N_l^0}{m a_0^3 \hbar \omega_{x,1}} = \frac{4\pi a_{jl} N_l^0}{a_0}, \quad j, l = 1, \dots, M, \\ B &= G_0^{-1} \hat{B} G_0, \quad \text{with} \quad G_0 = \text{diag} \left(\sqrt{N_1^0}, \dots, \sqrt{N_M^0} \right). \end{aligned}$$

The VGPEs (2.4) conserves the **normalization of the vector wave function** or the total number of particles

$$N(G_0 \Psi) = \int_{\mathbb{R}^3} \|G_0 \Psi(\mathbf{x}, t)\|_{l^2}^2 d\mathbf{x} = \sum_{j=1}^M \int_{\mathbb{R}^3} N_j^0 |\psi_j(\mathbf{x}, t)|^2 d\mathbf{x} = N^0, \quad t \geq 0. \quad (2.5)$$

When there is no external driven field, i.e. $f \equiv 0$ in (2.4), the VGPEs (2.4) is time reversible, time transverse invariant, and conserves the **normalization of the wave function for each component** or the number of particles of each component

$$N_j(\psi_j) = \int_{\mathbb{R}^3} |\psi_j(\mathbf{x}, t)|^2 d\mathbf{x} = 1, \quad t \geq 0, \quad j = 1, \dots, M \quad (2.6)$$

and the **energy**

$$E_\beta(\Psi) = \sum_{j=1}^M \frac{N_j^0}{N^0} E_{\beta,j}(\Psi), \quad (2.7)$$

with

$$\begin{aligned} N^0 &= N_1^0 + \dots + N_M^0, \quad \beta = \max_{1 \leq j, l \leq M} |\beta_{jl}|, \\ E_{\beta,j}(\Psi) &= \int_{\mathbb{R}^3} \left[\frac{1}{2} |\nabla \psi_j|^2 + V_j(\mathbf{x}) |\psi_j|^2 + \frac{1}{2} \sum_{l=1}^M \beta_{jl} |\psi_j|^2 |\psi_l|^2 \right] d\mathbf{x}, \quad j = 1, \dots, M. \end{aligned}$$

There are two extreme regimes: one is when $\beta \ll 1$ ($\iff |\beta_{jl}| \ll 1$ for all $j, l = 1, \dots, M$), then the system (2.4) describes a weakly interacting condensation. The other one is when $\beta \gg 1$, then (2.4) corresponds to a strongly interacting condensation or to the semiclassical regime or the Thomas-Fermi regime.

2.2 Reduction to lower dimensions

In the following two cases, the 3d VGPEs (2.4) without external driven field, i.e. $f \equiv 0$, can approximately be reduced to 2d or even 1d. In the case (disk-shaped condensation)

$$\omega_{x,j} \approx \omega_{y,j} \approx \omega_{x,1}, \quad \omega_{z,j} \gg \omega_{x,1} \quad \iff \quad \gamma_{x,j} \approx \gamma_{y,j} \approx 1, \quad \gamma_{z,j} \gg 1, \quad j = 1, \dots, M, \quad (2.8)$$

the 3d VGPEs (2.4) can be reduced to 2d VGPEs with $\mathbf{x} = (x, y)^T$ by assuming that the time evolution does not cause excitations along the z -axis since they have large energy of approximately $\hbar\omega_{z,j}$ compared to excitations along the x and y -axis with energies of about $\hbar\omega_{x,1}$. Thus we may assume that the condensate wave function along the z -axis is always well described by the ground state wave function and set

$$\Psi = \Psi_2(x, y, t) \dot{*} \Psi_3(z) \quad \text{with} \quad \Psi_3(z) = \left(\int_{\mathbb{R}^2} \Phi_g(x, y, z) \dot{*} \Phi_g^*(x, y, z) dx dy \right)^{1/2}, \quad (2.9)$$

where $\Psi_2(x, y, t) = (\psi_{2,1}(x, y, t), \dots, \psi_{2,M}(x, y, t))^T$, $\Psi_3(z) = (\psi_{3,1}(z), \dots, \psi_{3,M}(z))^T$ and $\Phi_g(x, y, z) = (\phi_{g,1}(x, y, z), \dots, \phi_{g,M}(x, y, z))^T$ (see detail in (3.5)) is the ground state solution of the 3d VGPEs (2.4) by setting $f \equiv 0$ and g^* denotes the conjugate of a function g . Plugging (2.9) into (2.4), then $\dot{*}$ both sides by $\Phi_3^*(z)$, integrating with respect to z over $(-\infty, \infty)$, we get

$$i \frac{\partial \Psi_2(\mathbf{x}, t)}{\partial t} = -\frac{1}{2} \nabla^2 \Psi_2(\mathbf{x}, t) + (\mathbf{V}(\mathbf{x}) + \mathbf{C}) \dot{*} \Psi_2(\mathbf{x}, t) + \mathbf{A}(\Psi_2) \dot{*} \Psi_2(\mathbf{x}, t), \quad (2.10)$$

where

$$\begin{aligned} \mathbf{V}(\mathbf{x}) &= (V_1(x, y), \dots, V_M(x, y))^T, \\ V_j(x, y) &= \frac{1}{2} \left(\gamma_{x,j}^2 (x - x_{0,j})^2 + \gamma_{y,j}^2 (y - y_{0,j})^2 \right), \quad j = 1, \dots, M, \\ \mathbf{C} &= (c_1, \dots, c_M)^T, \\ c_j &= \frac{\gamma_{z,j}^2}{2} \int_{-\infty}^{\infty} (z - z_{0,j})^2 |\psi_{3,j}|^2 dz + \frac{1}{2} \int_{-\infty}^{\infty} \left| \frac{d\psi_{3,j}(z)}{dz} \right|^2 dz, \quad j = 1, \dots, M, \\ \mathbf{A}(\Psi) &= (A_1(\Psi), \dots, A_M(\Psi))^T, \\ A_j(\Psi) &= \sum_{l=1}^M \left(\beta_{jl} \int_{-\infty}^{\infty} |\psi_{3,j}(z)|^2 |\psi_{3,l}(z)|^2 dz \right) |\psi_{2,l}|^2, \quad j = 1, \dots, M. \end{aligned}$$

Since this VGPEs is time-transverse invariant, we can replace $\Psi_2 \rightarrow \Psi_2 \dot{*} e^{-i\mathbf{C}t/2}$ which drops the constant vector \mathbf{C} in the trap potential and obtain the 2d VGPEs

with $\Psi = \Psi_2$ and $\mathbf{x} = (x, y)^T$

$$i \frac{\partial \Psi(\mathbf{x}, t)}{\partial t} = -\frac{1}{2} \nabla^2 \Psi(\mathbf{x}, t) + \mathbf{V}(\mathbf{x}) \dot{*} \Psi(\mathbf{x}, t) + \mathbf{A}(\Psi) \dot{*} \Psi(\mathbf{x}, t). \quad (2.11)$$

The observables are not affected by this.

Similarly in the case (cigar-shaped condensation)

$$\omega_{x,j} \approx \omega_{x,1}, \quad \omega_{y,j} \gg \omega_{x,1}, \quad \omega_{z,j} \gg \omega_{x,1} \iff \gamma_{x,j} \approx 1, \quad \gamma_{y,j} \gg 1, \quad \gamma_{z,j} \gg 1, \quad 1 \leq j \leq M, \quad (2.12)$$

the 3d VGPEs (2.4) can be reduced to 1d VGPEs with $\mathbf{x} = x$. Similarly to the 2d case, we derive the 1d VGPEs

$$i \frac{\partial \Psi(x, t)}{\partial t} = -\frac{1}{2} \nabla^2 \Psi(x, t) + \mathbf{V}(x) \dot{*} \Psi(x, t) + \mathbf{A}(\Psi) \dot{*} \Psi(x, t), \quad (2.13)$$

where

$$\begin{aligned} \mathbf{V}(x) &= (V_1(x), \dots, V_M(x))^T, \\ V_j(x) &= \frac{1}{2} \gamma_{x,j}^2 (x - x_{0,j})^2, \quad j = 1, \dots, M, \\ \mathbf{A}(\Psi) &= (A_1(\Psi), \dots, A_M(\Psi))^T, \\ A_j(\Psi) &= \sum_{l=1}^M \left(\beta_{jl} \int_{\mathbb{R}^2} |\psi_{23,j}(y, z)|^2 |\psi_{23,l}(y, z)|^2 dz \right) |\psi_l|^2, \\ \psi_{23,j}(y, z) &= \left(\int_{-\infty}^{\infty} |\phi_{g,j}(x, y, z)|^2 dx \right)^{1/2}, \quad j = 1, \dots, M. \end{aligned}$$

In fact, the 3d VGPEs (2.4), 2d VGPEs (2.11) and 1d VGPEs (2.13) with an external driven field can be written in a unified way

$$i \frac{\partial \Psi(\mathbf{x}, t)}{\partial t} = -\frac{1}{2} \nabla^2 \Psi(\mathbf{x}, t) + \mathbf{V}_d(\mathbf{x}) \dot{*} \Psi(\mathbf{x}, t) + \mathbf{A}_d(\Psi) \dot{*} \Psi(\mathbf{x}, t) + f(t) B \Psi(\mathbf{x}, t), \quad \mathbf{x} \in \mathbb{R}^d, \quad (2.14)$$

where

$$\begin{aligned} \mathbf{V}_d(\mathbf{x}) &= (V_{d,1}(\mathbf{x}), \dots, V_{d,M}(\mathbf{x}))^T, \\ \mathbf{A}_d(\Psi) &= (A_{d,1}(\Psi), \dots, A_{d,M}(\Psi))^T, \\ A_{d,j}(\Psi) &= \beta_{d,j1} |\psi_1|^2 + \dots + \beta_{d,jM} |\psi_M|^2, \quad j = 1, \dots, M; \end{aligned}$$

with

$$\begin{aligned} V_{d,j} &= \begin{cases} \frac{1}{2} \gamma_{x,j}^2 (x - x_{0,j})^2, & d = 1, \\ \frac{1}{2} \left(\gamma_{x,j}^2 (x - x_{0,j})^2 + \gamma_{y,j}^2 (y - y_{0,j})^2 \right), & d = 2, \\ \frac{1}{2} \left(\gamma_{x,j}^2 (x - x_{0,j})^2 + \gamma_{y,j}^2 (y - y_{0,j})^2 + \gamma_{z,j}^2 (z - z_{0,j})^2 \right), & d = 3; \end{cases} \\ \beta_{d,jl} &= \begin{cases} \beta_{jl} \int_{\mathbb{R}^2} |\psi_{23,j}|^2 |\psi_{23,l}|^2 dy dz, & d = 1, \\ \beta_{jl} \int_{-\infty}^{\infty} |\psi_{3,j}|^2 |\psi_{3,l}|^2 dz, & d = 2, \\ \beta_{jl}, & d = 3. \end{cases} \end{aligned}$$

The VGPEs (2.14) conserves the **normalization of the vector wave function** or the total number of particles

$$N(G_0\Psi) = \int_{\mathbb{R}^d} \|G_0\Psi(\mathbf{x}, t)\|_{l^2}^2 d\mathbf{x} = \sum_{j=1}^M \int_{\mathbb{R}^d} N_j^0 |\psi_j(\mathbf{x}, t)|^2 d\mathbf{x} = N^0, \quad t \geq 0. \quad (2.15)$$

When there is no external driven field, i.e. $f \equiv 0$ in (2.14), the VGPEs (2.14) is time reversible, time transverse invariant, and conserves the **normalization of the wave function for each component** or the number of particles of each component

$$N_j(\psi_j) = \int_{\mathbb{R}^d} |\psi_j(\mathbf{x}, t)|^2 d\mathbf{x} = 1, \quad t \geq 0, \quad j = 1, \dots, M \quad (2.16)$$

and the **energy**

$$E_\beta(\Psi) = \sum_{j=1}^M \frac{N_j^0}{N^0} E_{\beta,j}(\Psi), \quad (2.17)$$

with

$$E_{\beta,j}(\Psi) = \int_{\mathbb{R}^d} \left[\frac{1}{2} |\nabla \psi_j|^2 + V_{d,j}(\mathbf{x}) |\psi_j|^2 + \frac{1}{2} \sum_{l=1}^M \beta_{d,jl} |\psi_j|^2 |\psi_l|^2 \right] d\mathbf{x}, \quad j = 1, \dots, M.$$

3 Ground state solution

To find a stationary solution of (2.14) without external driven field, i.e. $f \equiv 0$, we write

$$\Psi(\mathbf{x}, t) = e^{-i\mathcal{U}t} \star \Phi(\mathbf{x}), \quad (3.1)$$

where $\mathcal{U} = (\mu_1, \dots, \mu_M)^T$ is the chemical potential vector of the multi-component condensate and $\Phi(\mathbf{x}) = (\phi_1(\mathbf{x}), \dots, \phi_M(\mathbf{x}))^T$ a real-valued vector function independent of time. Inserting (3.1) into (2.14) gives the following equations for (\mathcal{U}, Φ) :

$$\mathcal{U} \star \Phi(\mathbf{x}) = -\frac{1}{2} \Delta \Phi(\mathbf{x}) + \mathbf{V}_d(\mathbf{x}) \star \Phi(\mathbf{x}) + \mathbf{A}_d(\Phi) \star \Phi(\mathbf{x}), \quad \mathbf{x} \in \mathbb{R}^d, \quad (3.2)$$

under the normalization condition

$$\int_{\mathbb{R}^d} |\phi_j(\mathbf{x})|^2 d\mathbf{x} = 1, \quad j = 1, \dots, M. \quad (3.3)$$

This is a nonlinear eigenvalue problem under the constraint (3.3) and any eigenvalue vector \mathcal{U} can be computed from its corresponding eigenfunction vector Φ by

$$\begin{aligned} \mu_j &= \mu_{\beta,j}(\Phi) = \int_{\mathbb{R}^d} \left[\frac{1}{2} |\nabla \phi_j(\mathbf{x})|^2 + V_{d,j}(\mathbf{x}) |\phi_j(\mathbf{x})|^2 + \mathbf{A}_{d,j}(\Phi) |\phi_j(\mathbf{x})|^2 \right] d\mathbf{x} \\ &= \int_{\mathbb{R}^d} \left[\frac{1}{2} |\nabla \phi_j(\mathbf{x})|^2 + V_{d,j}(\mathbf{x}) |\phi_j(\mathbf{x})|^2 + \sum_{l=1}^M \beta_{d,jl} |\phi_l(\mathbf{x})|^2 |\phi_j(\mathbf{x})|^2 \right] d\mathbf{x} \\ &= E_{\beta,j}(\Phi) + \frac{1}{2} \int_{\mathbb{R}^d} \sum_{l=1}^M \beta_{d,jl} |\phi_l(\mathbf{x})|^2 |\phi_j(\mathbf{x})|^2 d\mathbf{x}, \quad j = 1, \dots, M. \end{aligned} \quad (3.4)$$

It is easy to see that critical points of the energy functional $E_\beta(\Phi)$ under the constraint (3.3) are eigenfunctions of the nonlinear eigenvalue problem (3.2) under the constraint (3.3) and versus versa. In fact, (3.2) can be viewed as the Euler-Lagrange equations of the energy functional $E_\beta(\Phi)$ under the constraint (3.3). The multi-component BEC ground state solution $\Phi_g(\mathbf{x})$ is found by minimizing the energy $E_\beta(\Phi)$ under the constraint (3.3), i.e.

(V) Find $(\mathcal{U}_g = (\mu_{g,1}, \dots, \mu_{g,M})^T, \Phi_g = (\phi_{g,1}, \dots, \phi_{g,M})^T \in \mathbf{U})$ such that

$$E_\beta(\Phi_g) = \min_{\Phi \in \mathbf{U}} E_\beta(\Phi), \quad (3.5)$$

$$\mu_{g,j} = \mu_{\beta,j}(\Phi_g) = E_{\beta,j}(\Phi_g) + \frac{1}{2} \int_{\mathbb{R}^d} \sum_{l=1}^M \beta_{d,jl} |\phi_{g,j}(\mathbf{x})|^2 |\phi_{g,l}(\mathbf{x})|^2 d\mathbf{x}, \quad 1 \leq j \leq M, \quad (3.6)$$

where the set \mathbf{U} is defined as

$$\mathbf{U} = \left\{ \Phi \mid E_\beta(\Phi) < \infty, \int_{\mathbb{R}^d} |\phi_j(\mathbf{x})|^2 d\mathbf{x} = 1, 1 \leq j \leq M \right\}.$$

In non-rotating multi-component BEC, the minimization problem (3.5) has a unique real-valued nonnegative ground state solution $\Phi_g(\mathbf{x}) > \mathbf{0}$ for $\mathbf{x} \in \mathbb{R}^d$ [38]. When $M = 1$, i.e. single-component BEC, the minimizer of (3.5) was computed by either a normalized gradient flow [4], or directly minimizing the energy functional [11], or the imaginary time method [1, 19], etc. Here we extend the normalized gradient flow method for computing ground state solution from single-component BEC to multi-component BEC.

3.1 Normalized gradient flow and energy diminishing

Consider the following continuous normalized gradient flow

$$\Phi_t = \frac{1}{2} \Delta \Phi - \mathbf{V}_d(\mathbf{x}) \dot{*} \Phi - \mathbf{A}_d(\Phi) \dot{*} \Phi + \mathcal{U}_\Phi(t) \dot{*} \Phi, \quad \mathbf{x} \in \mathbb{R}^d, t \geq 0, \quad (3.7)$$

$$\Phi(\mathbf{x}, 0) = \Phi_0(\mathbf{x}) = (\phi_{0,1}(\mathbf{x}), \dots, \phi_{0,M}(\mathbf{x}))^T, \quad \mathbf{x} \in \mathbb{R}^d; \quad (3.8)$$

where $\mathcal{U}_\Phi(t) = (\mu_{\Phi,1}(t), \dots, \mu_{\Phi,M}(t))^T$ with

$$\begin{aligned} \mathcal{U}_{\Phi,j}(t) = & \frac{1}{\|\phi_j(\cdot, t)\|^2} \int_{\mathbb{R}^d} \left[\frac{1}{2} |\nabla \phi_j(\mathbf{x}, t)|^2 + V_{d,j}(\mathbf{x}) |\phi_j(\mathbf{x}, t)|^2 \right. \\ & \left. + \sum_{l=1}^M \beta_{d,jl} |\phi_l(\mathbf{x}, t)|^2 |\phi_j(\mathbf{x}, t)|^2 \right] d\mathbf{x}, \quad j = 1, \dots, M. \end{aligned} \quad (3.9)$$

In fact, the right hand side of (3.7) is the same as (3.2) if we view $\mathcal{U}_\Phi(t)$ as a Lagrange multiplier for the constraint (3.3). Furthermore, as observed in [4] for single-component BEC, the solution of (3.7) also satisfies the following theorem:

Theorem 3.1 Suppose $\mathbf{V}_d(\mathbf{x}) \geq \mathbf{0}$ for all $\mathbf{x} \in \mathbb{R}^d$, $\beta_{jl} \geq 0$ ($j, l = 1, \dots, M$) and $\|\phi_{0,j}\| = 1$ ($j = 1, \dots, M$). Then the normalized gradient flow (3.7)-(3.8) is normalization conservation and energy diminishing, i.e.

$$\|\phi_j(\cdot, t)\|^2 = \int_{\mathbb{R}^d} \phi_j^2(\mathbf{x}, t) d\mathbf{x} = \|\phi_{0,j}\|^2 = 1, \quad t \geq 0, \quad j = 1, \dots, M, \quad (3.10)$$

$$\frac{d}{dt} E_\beta(\Phi) = - \sum_{j=1}^M \frac{2N_j^0}{N^0} \|\partial_t \phi_j(\cdot, t)\|^2 = - \sum_{j=1}^M \frac{2N_j^0}{N^0} \int_{\mathbb{R}^d} |\partial_t \phi_j(\mathbf{x}, t)|^2 d\mathbf{x} \leq 0, \quad t \geq 0, \quad (3.11)$$

which in turn implies

$$E_\beta(\Phi(\cdot, t_1)) \geq E_\beta(\Phi(\cdot, t_2)), \quad 0 \leq t_1 \leq t_2 < \infty.$$

Proof: Multiplying the j th ($j = 1, \dots, M$) equation in (3.7) by ϕ_j , integrating over \mathbb{R}^d , integration by parts and notice (3.9), we obtain

$$\begin{aligned} & \frac{1}{2} \frac{d}{dt} \int_{\mathbb{R}^d} \phi_j^2(\mathbf{x}, t) d\mathbf{x} = \int_{\mathbb{R}^d} \phi_j \partial_t \phi_j d\mathbf{x} \\ & = \int_{\mathbb{R}^d} \left[\frac{1}{2} \Delta \phi_j - V_{d,j}(\mathbf{x}) \phi_j - A_{d,j}(\Phi) \phi_j + \mu_{\Phi,j}(t) \phi_j \right] \phi_j d\mathbf{x} \\ & = - \int_{\mathbb{R}^d} \left[\frac{1}{2} |\nabla \phi_j(\mathbf{x}, t)|^2 + V_{d,j}(\mathbf{x}) \phi_j^2(\mathbf{x}, t) + A_{d,j}(\Phi) \phi_j^2 \right] d\mathbf{x} + \mu_{\Phi,j}(t) \|\phi_j(\cdot, t)\|^2 \\ & = 0, \quad t \geq 0, \quad j = 1, \dots, M. \end{aligned} \quad (3.12)$$

This implies the normalization conservation (3.10).

Next, direct calculation shows

$$\begin{aligned} \frac{d}{dt} E_\beta(\Phi) &= \sum_{j=1}^M \frac{N_j^0}{N^0} \frac{d}{dt} E_{\beta,j}(\Phi) \\ &= \sum_{j=1}^M \frac{N_j^0}{N^0} \int_{\mathbb{R}^d} \left[\nabla \phi_j \cdot \nabla (\partial_t \phi_j) + 2V_{d,j}(\mathbf{x}) \phi_j \partial_t \phi_j + \sum_{l=1}^M \beta_{jl} \left(|\phi_l|^2 \phi_j \partial_t \phi_j + |\phi_j|^2 \phi_l \partial_t \phi_l \right) \right] d\mathbf{x} \\ &= \sum_{j=1}^M \frac{N_j^0}{N^0} \int_{\mathbb{R}^d} \left[\nabla \phi_j \cdot \nabla (\partial_t \phi_j) + 2V_{d,j}(\mathbf{x}) \phi_j \partial_t \phi_j + \sum_{l=1}^M \beta_{jl} |\phi_l|^2 \phi_j \partial_t \phi_j \right] d\mathbf{x} \\ &\quad + \sum_{j=1}^M \sum_{l=1}^M \frac{N_j^0}{N^0} \int_{\mathbb{R}^d} \beta_{jl} |\phi_j|^2 \phi_l \partial_t \phi_l d\mathbf{x} \\ &= \sum_{j=1}^M \frac{N_j^0}{N^0} \int_{\mathbb{R}^d} \left[\nabla \phi_j \cdot \nabla (\partial_t \phi_j) + 2V_{d,j}(\mathbf{x}) \phi_j \partial_t \phi_j + \sum_{l=1}^M \beta_{jl} |\phi_l|^2 \phi_j \partial_t \phi_j \right] d\mathbf{x} \\ &\quad + \sum_{l=1}^M \frac{N_l^0}{N^0} \sum_{j=1}^M \int_{\mathbb{R}^d} \beta_{lj} |\phi_j|^2 \phi_l \partial_t \phi_l d\mathbf{x} \end{aligned}$$

$$\begin{aligned}
&= \sum_{j=1}^M \frac{2N_j^0}{N^0} \int_{\mathbb{R}^d} \left[\nabla \phi_j \cdot \nabla (\partial_t \phi_j) + 2V_{d,j}(\mathbf{x}) \phi_j \partial_t \phi_j + \sum_{l=1}^M \beta_{jl} |\phi_l|^2 \phi_j \partial_t \phi_j \right] d\mathbf{x} \\
&= 2 \int_{\mathbb{R}^d} \left[-\frac{1}{2} \Delta \phi_j + V_{d,j}(\mathbf{x}) \phi_j + A_{d,j}(\Phi) \phi_j \right] \partial_t \phi_j d\mathbf{x} \\
&= \sum_{j=1}^M \frac{2N_j^0}{N^0} \int_{\mathbb{R}^d} [-\partial_t \phi_j(\mathbf{x}, t) + \mu_{\Phi,j}(t) \phi_j(\mathbf{x}, t)] \partial_t \phi_j d\mathbf{x} \\
&= -\sum_{j=1}^M \frac{2N_j^0}{N^0} \|\partial_t \phi_j(\cdot, t)\|^2 + \mu_{\Phi,j}(t) \frac{d}{dt} \int_{\mathbb{R}^d} |\phi_j(\mathbf{x}, t)|^2 d\mathbf{x} \\
&= -\sum_{j=1}^M \frac{2N_j^0}{N^0} \|\partial_t \phi_j(\cdot, t)\|^2, \quad t \geq 0, \tag{3.13}
\end{aligned}$$

since $\mu_{\Phi,j}(t)$ ($j = 1, \dots, M$) are always real and

$$\frac{d}{dt} \int_{\mathbb{R}^d} |\phi_j(\mathbf{x}, t)|^2 d\mathbf{x} = 0, \quad j = 1, \dots, M$$

due to the normalization conservation. Thus, we easily get

$$E_\beta(\Phi(\cdot, t_1)) \geq E_\beta(\Phi(\cdot, t_2)), \quad 0 \leq t_1 \leq t_2 < \infty$$

for the solution of (3.7). \square

Using argument similar to that in [46], we may also get as $t \rightarrow \infty$, Φ approaches to a steady state solution which is a critical point of the energy. In non-rotating multi-component BEC, it has a unique real valued nonnegative ground state solution $\Phi_g(\mathbf{x}) \geq 0$ for all $\mathbf{x} \in \mathbb{R}^d$ [38]. We choose the initial data $\Phi_0(\mathbf{x}) \geq 0$ for $\mathbf{x} \in \mathbb{R}^d$, e.g. the approximate ground state solution (3.33) in weakly interacting multi-component BEC. Under this kind of initial data, the ground state solution Φ_g and its corresponding chemical potential \mathcal{U}_g can be obtained from the steady state solution of the normalized gradient flow (3.7)-(3.8), i.e.

$$\Phi_g(\mathbf{x}) = \lim_{t \rightarrow \infty} \Phi(\mathbf{x}, t), \quad \mathbf{x} \in \mathbb{R}^d, \tag{3.14}$$

$$\mu_{g,j} = \mu_{\beta,j}(\Phi_g) = E_\beta(\Phi_g) + \frac{1}{2} \int_{\mathbb{R}^d} \sum_{l=1}^M \beta_{d,jl} |\phi_{g,l}(\mathbf{x})|^2 |\phi_{g,j}(\mathbf{x})|^2 d\mathbf{x}, \quad j = 1, \dots, M. \tag{3.15}$$

3.2 Projection

When one wants to evolve the normalized gradient flow (3.7), (3.8) numerically, it is natural to consider the following projection (or splitting) scheme which was widely used in physical literatures for computing the ground state solution of single-component BEC [4] by constructing a time sequence $0 = t_0 < t_1 < t_2 < \dots < t_n < \dots$ with $t_n = n k$ and $k > 0$ time step:

$$\Phi_t = \frac{1}{2} \Delta \Phi - \mathbf{V}_d(\mathbf{x}) \ast \Phi - \mathbf{A}_d(\Phi) \ast \Phi, \quad \mathbf{x} \in \mathbb{R}^d, \quad t_n \leq t < t_{n+1}, \quad n \geq 0, \tag{3.16}$$

$$\phi_j(\mathbf{x}, t_{n+1}) \triangleq \phi_j(\mathbf{x}, t_{n+1}^+) = \frac{\phi_j(\mathbf{x}, t_{n+1}^-)}{\|\phi_j(\cdot, t_{n+1}^-)\|}, \quad \mathbf{x} \in \mathbb{R}^d, \quad n \geq 0, \quad (3.17)$$

$$\Phi(\mathbf{x}, 0) = \Phi_0(\mathbf{x}), \quad \mathbf{x} \in \mathbb{R}^d; \quad (3.18)$$

where $\Phi(\mathbf{x}, t_n^\pm) = (\phi_1(\mathbf{x}, t_n^\pm), \dots, \phi_M(\mathbf{x}, t_n^\pm))^T = \lim_{t \rightarrow t_n^\pm} \Phi(\mathbf{x}, t)$ and $\|\phi_{0,j}\| = 1$ ($j = 1, \dots, M$). In fact, the gradient flow with projection (3.16), (3.17) can be viewed as applying the steepest decent method to the minimization problem (3.5) by ignoring the constraint $\Phi \in \mathbf{U}$ and then projecting back to the set \mathbf{U} . The gradient flow (3.16) can also be viewed as applying an imaginary time (i.e. $t \rightarrow -it$) in (2.14). The normalized step (3.17) is equivalent to solving the following ODE system *exactly*

$$\Phi_t(\mathbf{x}, t) = \mathcal{U}_\Phi(t, k) \dot{\ast} \Phi(\mathbf{x}, t), \quad \mathbf{x} \in \mathbb{R}^d, \quad t_n \leq t < t_{n+1}, \quad n \geq 0, \quad (3.19)$$

$$\Phi(\mathbf{x}, t_n^+) = \Phi(\mathbf{x}, t_{n+1}^-), \quad \mathbf{x} \in \mathbb{R}^d; \quad (3.20)$$

where $\mathcal{U}_\Phi(t, k) = (\mu_{\Phi,1}(t, k), \dots, \mu_{\Phi,M}(t, k))^T$ with

$$\mu_{\Phi,j}(t, k) \equiv \mu_{\Phi,j}(t_{n+1}, k) = -\frac{1}{2k} \ln \|\phi_j(\cdot, t_{n+1}^-)\|^2, \quad t_n \leq t \leq t_{n+1}, \quad j = 1, \dots, M. \quad (3.21)$$

Thus the gradient flow with projection can be viewed as a first-order splitting method for the following continuous gradient flow with discontinuous coefficients:

$$\Phi_t = \frac{1}{2} \Delta \Phi - \mathbf{V}_d(\mathbf{x}) \dot{\ast} \Phi - \mathbf{A}_d(\Phi) \dot{\ast} \Phi + \mathcal{U}_\Phi(t, k) \dot{\ast} \Phi, \quad \mathbf{x} \in \mathbb{R}^d, \quad n \geq 0, \quad (3.22)$$

$$\Phi(\mathbf{x}, 0) = \Phi_0(\mathbf{x}), \quad \mathbf{x} \in \mathbb{R}^d; \quad (3.23)$$

Let $k \rightarrow 0$, note (3.21) and (3.16), we see that

$$\begin{aligned} \mu_{\Phi,j}(t) &= \lim_{k \rightarrow 0^+} \mu_{\Phi,j}(t, k) = \frac{1}{\|\phi_j(\cdot, t)\|^2} \int_{\mathbb{R}^d} \left[\frac{1}{2} |\nabla \phi_j(\mathbf{x}, t)|^2 + V_{d,j}(\mathbf{x}) |\phi_j(\mathbf{x}, t)|^2 \right. \\ &\quad \left. + \sum_{l=1}^M \beta_{d,jl} |\phi_l(\mathbf{x}, t)|^2 |\phi_j(\mathbf{x}, t)|^2 \right] d\mathbf{x}, \quad j = 1, \dots, M, \end{aligned} \quad (3.24)$$

which implies that the problem of (3.22), (3.23) collapses to (3.16), (3.17) as $k \rightarrow 0$. Furthermore, using the Theorem 2.1 in [4], we get immediately

Theorem 3.2 *Suppose $\mathbf{V}_d(\mathbf{x}) \geq \mathbf{0}$ for all $\mathbf{x} \in \mathbb{R}^d$ and $\|\phi_{0,j}\| = 1$ ($j = 1, \dots, M$). For $\beta_{jl} = 0$ ($j, l = 1, \dots, M$), the gradient flow with projection (3.16)-(3.18) is energy diminishing under any time step k and initial data Φ_0 , i.e.*

$$E_0(\Phi(\cdot, t_{n+1})) \leq E_0(\Phi(\cdot, t_n)) \leq \dots \leq E_0(\Phi(\cdot, 0)) = E_0(\Phi_0), \quad n = 0, 1, 2, \dots. \quad (3.25)$$

3.3 Backward Euler finite difference (BEFD) discretization

In this subsection, we present a fully discretization of the gradient flow with projection (3.16), (3.17) by the backward Euler finite difference (BEFD) which was proposed in [4] for discretizing a normalized gradient flow for single-component BEC.

For simplicity of notation we shall introduce the method for the case of one spatial dimension ($d = 1$) with homogeneous Dirichlet boundary conditions. Generalizations to $d > 1$ are straightforward for tensor product grids and the results remain valid without modifications. For $d = 1$, the problem becomes

$$\Phi_t = \frac{1}{2}\Phi_{xx} - \mathbf{V}_1(x) \dot{\ast} \Phi - \mathbf{A}_1(\Phi) \dot{\ast} \Phi, \quad a < x < b, \quad t_n \leq t < t_{n+1}, \quad n \geq 0, \quad (3.26)$$

$$\phi_j(x, t_{n+1}) \triangleq \phi_j(x, t_{n+1}^+) = \frac{\phi_j(x, t_{n+1}^-)}{\|\phi_j(\cdot, t_{n+1}^-)\|}, \quad a \leq x \leq b, \quad n \geq 0, \quad j = 1, \dots, M, \quad (3.27)$$

$$\Phi(x, 0) = \Phi_0(x), \quad a \leq x \leq b, \quad (3.28)$$

$$\Phi(a, t) = \Phi(b, t) = \mathbf{0}, \quad t \geq 0; \quad (3.29)$$

with

$$\|\phi_{0,j}\|^2 = \int_a^b \phi_{0,j}^2(x) dx = 1, \quad j = 1, \dots, M.$$

We choose the spatial mesh size $h = \Delta x > 0$ with $h = (b - a)/N$ and N an even positive integer, and define grid points by

$$x_j := a + j h, \quad j = 0, 1, \dots, N.$$

Let $\Phi_j^n = ((\phi_1)_j^n, \dots, (\phi_M)_j^n)^T$ be the numerical approximation of $\Phi(x_j, t_n) = (\phi_1(x_j, t_n), \dots, \phi_M(x_j, t_n))^T$. Here we use the backward Euler for time discretization and second-order centered finite difference for spatial derivatives for the gradient flow (3.16). The detail scheme is:

$$\begin{aligned} \frac{\Phi_j^* - \Phi_j^n}{k} &= \frac{1}{2h^2} [\Phi_{j+1}^* - 2\Phi_j^* + \Phi_{j-1}^*] - \mathbf{V}_1(x_j) \dot{\ast} \Phi_j^* - \mathbf{A}_1(\Phi_j^n) \dot{\ast} \Phi_j^*, \\ & \quad j = 1, \dots, N-1, \\ \Phi_0^* &= \Phi_N^* = 0, \\ (\phi_l)_j^{n+1} &= \frac{(\phi_l)_j^*}{\sqrt{h \sum_{s=1}^{N-1} ((\phi_l)_s^*)^2}}, \quad j = 0, \dots, N, \quad l = 1, \dots, M, \quad n = 0, 1, \dots, \\ \Phi_j^0 &= \Phi_0(x_j), \quad j = 0, 1, \dots, N. \end{aligned} \quad (3.30)$$

It is easy to see that the discretization BEFD (3.30) is monotone for any time step $k > 0$ when $\mathbf{V}_1(\mathbf{x}) \geq \mathbf{0}$ and $\beta_{jl} \geq 0$ ($j, l = 1, \dots, M$). Furthermore, similar to the proof of Theorem 3.1 in [4], we can prove the BEFD normalized flow (3.30) is energy diminishing for any time step $k > 0$ when $\mathbf{V}_1(\mathbf{x}) \geq \mathbf{0}$ and $\beta_{jl} = 0$ ($j, l = 1, \dots, M$).

Remark 3.1 *Extension of the BEFD discretization (3.26) for mutli-component BEC can be done as those in the Appendix in [4] for single-component BEC in the cases when $\mathbf{V}_d(\mathbf{x})$ in 2d with radial symmetry or in 3d with spherical symmetry or cylindrical symmetry, as well as in 2d or 3d for central vortex states.*

3.4 Approximate ground state solution

For a weakly interacting condensate, i.e. $\beta \ll 1$ ($\iff |\beta_{jl}| \ll 1$, $j, l = 1, \dots, M$), we drop the nonlinear terms (i.e. the last term on the right hand side of (3.2)) and find the linear vector Schrödinger equations with the harmonic oscillator potentials

$$\mathcal{U} \dot{*} \Phi(\mathbf{x}) = -\frac{1}{2} \Delta \Phi(\mathbf{x}) + \mathbf{V}_d(\mathbf{x}) \dot{*} \Phi(\mathbf{x}), \quad \mathbf{x} = (x_1, \dots, x_d)^T \in \mathbb{R}^d, \quad (3.31)$$

under the normalization condition (3.3). The ground state solution of (3.31) is [37]

$$\mu_{g,j}^w = \frac{\gamma_{x_1,j} + \dots + \gamma_{x_d,j}}{2}, \quad j = 1, \dots, M, \quad (3.32)$$

$$\phi_{g,j}^w(\mathbf{x}) = \frac{(\gamma_{x_1,j} \dots \gamma_{x_d,j})^{1/4}}{\pi^{d/4}} e^{-(\gamma_{x_1,j}(x_1 - (x_1)_{0,j})^2 + \dots + \gamma_{x_d,j}(x_d - (x_d)_{0,j})^2)/2}. \quad (3.33)$$

It can be viewed as an approximate ground state solution of (3.2) in the case of a weakly interacting multi-component BEC. This approximate ground state can be used as initial data in the normalized gradient flow (3.7), or (3.16) and (3.17), or (3.22) for computing the ground state solution of multi-component BEC when $\beta_{jl} \neq 0$.

3.5 Application to a two-state model

The normalized gradient flow method and its BEFD discretization for multi-component BEC can be applied to compute coupled basis wavefunctions with lowest energy of the nonlinear two-state model used in [14, 15] for studying vortex dynamics in single-component BEC with (or without) an external rotation. For the continece of the reader, here we briefly review the derivation of the nonlinear two-state model from the Gross-Pitaevskii equation (GPE). Consider the dimensionless GPE for BEC in 2d with radial symmetry [4, 11, 6]:

$$i \psi_t(r, \theta, t) = -\frac{1}{2} \left[\frac{1}{r} \frac{\partial}{\partial r} \left(r \frac{\partial \psi}{\partial r} \right) + \frac{\partial^2 \psi}{\partial \theta^2} \right] + \frac{r^2}{2} \psi + \beta |\psi|^2 \psi, \quad (3.34)$$

under the normalization condition

$$\int_0^\infty \int_0^{2\pi} |\psi(r, \theta, t)|^2 r dr d\theta = 1,$$

where (r, θ) is the polar coordinate, $\psi(r, \theta, t)$ is the macroscopic wave function for the condensate, β is a parameter models the interaction. In order to represent the condensate mean-field wavefunction ψ by the superposition of a symmetric component ϕ_s and a vortex component $\phi_v e^{i\theta}$, we take the ansatz

$$\psi(r, \theta, t) = a_s \phi_s(r; n_v) e^{-i\mu_s t} + a_v \phi_v(r; n_v) e^{i\theta} e^{-i\mu_v t}, \quad (3.35)$$

where a_s and a_v are the complex amplitudes of the symmetric and vortex components, respectively. The vortex fraction is $0 \leq n_v = |a_v|^2 \leq 1$ and the symmetric

fraction is $n_s = |a_s|^2 = 1 - n_v$. The ϕ_s and ϕ_v are real nonnegative functions, and are normalized to unity, i.e.

$$2\pi \int_0^\infty |\phi_s(r; n_v)|^2 r dr = 1, \quad 2\pi \int_0^\infty |\phi_v(r; n_v)|^2 r dr = 1. \quad (3.36)$$

Plugging (3.35) into (2.10), multiplying both sides by 1 and $e^{-i\theta}$, respectively, and then integrating over \mathbb{R}^2 , see detail in [14], we get the following nonlinear two-state model

$$\mu_s \phi_s = -\frac{1}{2r} \frac{d}{dr} \left(r \frac{d\phi_s}{dr} \right) + \frac{r^2}{2} \phi_s + \beta (n_s \phi_s^2 + 2F n_v \phi_v^2) \phi_s, \quad (3.37)$$

$$\mu_v \phi_v = -\frac{1}{2r} \frac{d}{dr} \left(r \frac{d\phi_v}{dr} \right) + \left(\frac{r^2}{2} + \frac{1}{2r^2} \right) \phi_v + \beta (2F n_s \phi_s^2 + n_v \phi_v^2) \phi_v, \quad (3.38)$$

$$\left. \frac{d\phi_s(r; n_v)}{dt} \right|_{r=0} = 0, \quad \phi_v(0; n_v) = 0, \quad \lim_{r \rightarrow \infty} \phi_s(r; n_v) = \lim_{r \rightarrow \infty} \phi_v(r; n_v) = 0; \quad (3.39)$$

where the factor $F = 1$, but can be adjusted in some cases. In order to study vortex dynamics in BEC through the two-state model (3.37), (3.38) [14, 15], one needs to find the coupled basis wavefunctions $\phi_s(r; n_v)$ and $\phi_v(r; n_v)$ for any given $0 \leq n_v \leq 1$ by minimizing the energy $E(\phi_s, \phi_v)$ defined as

$$E(\phi_s, \phi_v) = n_s E_s(\phi_s, \phi_v) + n_v E_v(\phi_s, \phi_v), \quad (3.40)$$

$$\begin{aligned} E_s(\phi_s, \phi_v) &= 2\pi \int_0^\infty \frac{r}{2} \left[\left| \frac{d\phi_s(r; n_v)}{dr} \right|^2 + r^2 \phi_s^2(r; n_v) \right. \\ &\quad \left. + \beta (n_s \phi_s^2(r; n_v) + 2F n_v \phi_v^2(r; n_v)) \phi_s^2(r; n_v) \right] dr, \\ E_v(\phi_s, \phi_v) &= 2\pi \int_0^\infty \frac{r}{2} \left[\left| \frac{d\phi_v(r; n_v)}{dr} \right|^2 + \left(r^2 + \frac{1}{r^2} \right) \phi_v^2(r; n_v) \right. \\ &\quad \left. + \beta (2F n_s \phi_s^2(r; n_v) + n_v \phi_v^2(r; n_v)) \phi_v^2(r; n_v) \right] dr; \end{aligned} \quad (3.41)$$

under the constraint (3.36). The continuous normalized gradient flow for computing the above minimizer is:

$$\frac{\partial \phi_s(r, t; n_v)}{\partial t} = \frac{1}{2r} \frac{d}{dr} \left(r \frac{d\phi_s}{dr} \right) - \frac{r^2}{2} \phi_s - \beta (n_s \phi_s^2 + 2F n_v \phi_v^2) \phi_s + \mu_s(t) \phi_s, \quad (3.42)$$

$$\frac{\partial \phi_v(r, t; n_v)}{\partial t} = \frac{1}{2r} \frac{d}{dr} \left(r \frac{d\phi_v}{dr} \right) - \left(\frac{r^2}{2} + \frac{1}{2r^2} \right) \phi_v - \beta (2F n_s \phi_s^2 + n_v \phi_v^2) \phi_v + \mu_v(t) \phi_v, \quad (3.43)$$

$$\left. \frac{\partial \phi_s(r, t; n_v)}{\partial t} \right|_{r=0} = 0, \quad \phi_v(0, t; n_v) = 0, \quad \lim_{r \rightarrow \infty} \phi_s(r, t; n_v) = \lim_{r \rightarrow \infty} \phi_v(r, t; n_v) = 0, \quad (3.44)$$

$$\phi_s(r, 0; n_v) = \phi_{s,0}(r) \geq 0, \quad \phi_v(r, 0; n_v) = \phi_{v,0}(r) \geq 0, \quad 0 \leq r < \infty; \quad (3.45)$$

with

$$2\pi \int_0^\infty |\phi_{s,0}(r)|^2 r dr = 1, \quad 2\pi \int_0^\infty |\phi_{v,0}(r)|^2 r dr = 1$$

and

$$\begin{aligned} \mu_s(t) &= \frac{1}{\int_0^\infty r |\phi_s(r, t; n_v)|^2 dr} \int_0^\infty \frac{r}{2} \left[\left| \frac{d\phi_s(r, t; n_v)}{dr} \right|^2 + r^2 \phi_s^2(r, t; n_v) \right. \\ &\quad \left. + 2\beta \left(n_s \phi_s^2(r, t; n_v) + 2Fn_v \phi_v^2(r, t; n_v) \right) \phi_s^2(r, t; n_v) \right] dr, \\ \mu_v(t) &= \frac{1}{\int_0^\infty r |\phi_v(r, t; n_v)|^2 dr} \int_0^\infty \frac{r}{2} \left[\left| \frac{d\phi_v(r, t; n_v)}{dr} \right|^2 + \left(r^2 + \frac{1}{r^2} \right) \phi_v^2(r, t; n_v) \right. \\ &\quad \left. + 2\beta \left(2Fn_s \phi_s^2(r, t; n_v) + n_v \phi_v^2(r, t; n_v) \right) \phi_v^2(r, t; n_v) \right] dr. \end{aligned}$$

If we choose the initial data $\phi_{s,0}(r) \geq 0$ and $\phi_{v,0}(r) \geq 0$ for $0 \leq r < \infty$, e.g. $\phi_{s,0}(r) = \frac{1}{\pi^{1/2}} e^{-r^2/2}$ and $\phi_{v,0}(r) = \frac{r}{\pi^{1/2}} e^{-r^2/2}$, then the minimizer $\phi_{s,g}(r; n_v)$ and $\phi_{v,g}(r; n_v)$ can be obtained from the steady state solution of the normalized gradient flow (3.42)-(3.45), i.e.

$$\begin{aligned} \phi_{s,g}(r; n_v) &= \lim_{t \rightarrow \infty} \phi_s(r, t; n_v), \quad \phi_{v,g}(r; n_v) = \lim_{t \rightarrow \infty} \phi_v(r, t; n_v), \quad 0 \leq r < \infty; \\ \mu_{s,g} &= 2\pi \int_0^\infty \frac{r}{2} \left[\left| \frac{d\phi_{s,g}(r; n_v)}{dr} \right|^2 + r^2 \phi_{s,g}^2(r; n_v) \right. \\ &\quad \left. + 2\beta \left(n_s \phi_{s,g}^2(r; n_v) + 2Fn_v \phi_{v,g}^2(r; n_v) \right) \phi_{s,g}^2(r; n_v) \right] dr, \\ \mu_{v,g} &= 2\pi \int_0^\infty \frac{r}{2} \left[\left| \frac{d\phi_{v,g}(r; n_v)}{dr} \right|^2 + \left(r^2 + \frac{1}{r^2} \right) \phi_{v,g}^2(r; n_v) \right. \\ &\quad \left. + 2\beta \left(2Fn_s \phi_{s,g}^2(r; n_v) + n_v \phi_{v,g}^2(r; n_v) \right) \phi_{v,g}^2(r; n_v) \right] dr. \end{aligned}$$

Choose $R > 0$ sufficiently large, denote the mesh size $h_r = (R - 0)/N$, grid points $r_j = j h_r$, $j = 0, 1, \dots, N$, and $r_{j-\frac{1}{2}} = \left(j - \frac{1}{2} \right) h_r$, $j = 0, 1, \dots, N + 1$. Then the BEFD discretization of the normalized gradient flow (3.42)-(3.45) reads:

$$\begin{aligned} \frac{(\phi_s)_{j-\frac{1}{2}}^* - (\phi_s)_{j-\frac{1}{2}}^n}{k} &= \frac{1}{2 h_r^2 r_{j-\frac{1}{2}}} \left[r_j (\phi_s)_{j+\frac{1}{2}}^* - (r_j + r_{j-1}) (\phi_s)_{j-\frac{1}{2}}^* + r_{j-1} (\phi_s)_{j-\frac{3}{2}}^* \right] - \frac{r_{j-\frac{1}{2}}^2}{2} (\phi_s)_{j-\frac{1}{2}}^* \\ &\quad - \beta \left[n_s ((\phi_s)_{j-\frac{1}{2}}^n)^2 + 2Fn_v \left(\frac{(\phi_v)_{j-1}^n + (\phi_v)_j^n}{2} \right)^2 \right] (\phi_s)_{j-\frac{1}{2}}^*, \quad j = 1, \dots, N, \\ \frac{(\phi_v)_j^* - (\phi_v)_j^n}{k} &= \frac{1}{2 h_r^2 r_j} \left[r_{j+\frac{1}{2}} (\phi_v)_{j+1}^* - \left(r_{j+\frac{1}{2}} + r_{j-\frac{1}{2}} \right) (\phi_v)_j^* + r_{j-\frac{1}{2}} (\phi_v)_{j-1}^* \right] - \left(\frac{r_j^2}{2} + \frac{1}{2r_j^2} \right) (\phi_v)_j^* \\ &\quad - \beta \left[2Fn_s \left(\frac{(\phi_s)_{j-\frac{1}{2}}^n + (\phi_s)_{j+\frac{1}{2}}^n}{2} \right)^2 + n_v ((\phi_v)_j^n)^2 \right] (\phi_v)_j^*, \quad j = 1, \dots, N - 1, \end{aligned}$$

$$\begin{aligned}
(\phi_s)_{-\frac{1}{2}}^* &= (\phi_s)_{\frac{1}{2}}^*, & (\phi_s)_{N+\frac{1}{2}}^* &= 0, & (\phi_v)_0^* &= (\phi_v)_N^* = 0, \\
(\phi_s)_{j-\frac{1}{2}}^{n+1} &= \frac{(\phi_s)_{j-\frac{1}{2}}^*}{\sqrt{h_r 2\pi \sum_{l=1}^N r_{j-\frac{1}{2}} \left((\phi_s)_{l-\frac{1}{2}}^* \right)^2}}, & j &= 0, \dots, N+1, & n &= 0, 1, \dots,
\end{aligned} \tag{3.46}$$

$$(\phi_v)_j^{n+1} = \frac{(\phi_v)_j^*}{\sqrt{2\pi h_r \sum_{l=1}^{N-1} r_j \left((\phi_s)_l^* \right)^2}}, \quad j = 0, \dots, N, \quad n = 0, 1, \dots, \tag{3.47}$$

$$\begin{aligned}
(\phi_s)_{j-\frac{1}{2}}^0 &= \phi_{s,0}(r_{j-\frac{1}{2}}), & j &= 1, \dots, N+1, & (\phi_s)_{-\frac{1}{2}}^0 &= (\phi_s)_{\frac{1}{2}}^0, \\
(\phi_v)_j^0 &= \phi_{v,0}(r_j), & j &= 0, 1, \dots, N.
\end{aligned}$$

Remark 3.2 *The normalized gradient flow and its BEFD discretization for the two-state model in 2d with radial symmetry can be easily extended to the two-state model in [15] in 3d with cylindrical symmetry.*

4 TSSP method for dynamics

In this section we present a time-splitting sine-spectral (TSSP) method for the VGPEs (2.14) with (or without) an external driven field for dynamics of multi-component BEC. For simplicity of notation we shall introduce the method in one space dimension ($d = 1$). Generalizations to $d > 1$ are straightforward for tensor product grids and the results remain valid without modifications. For $d = 1$, the equations (2.4) with homogeneous Dirichlet boundary conditions become

$$i \frac{\partial \Psi(x, t)}{\partial t} = -\frac{1}{2} \Psi_{xx}(x, t) + \mathbf{V}_1(x) * \Psi(x, t) + \mathbf{A}_1(\Psi) * \Psi(x, t) + f(t) B \Psi(x, t),$$

$$a < x < b, \quad t \geq 0, \tag{4.1}$$

$$\Psi(a, t) = \Psi(b, t) = \mathbf{0}, \quad t \geq 0, \tag{4.2}$$

$$\Psi(x, t = 0) = \Psi_0(x) = (\psi_{0,1}(x), \dots, \psi_{0,M}(x))^T, \quad a \leq x \leq b, \tag{4.3}$$

with

$$\|\psi_{0,j}\| = \int_a^b |\psi_{0,j}(x)|^2 dx = 1, \quad j = 1, \dots, M.$$

We choose the spatial mesh size $h = \Delta x > 0$ with $h = (b - a)/N$ for N an even positive integer, the time step $k = \Delta t > 0$ and let the grid points and the time step be

$$x_j := a + j h, \quad t_n := n k, \quad j = 0, 1, \dots, N, \quad n = 0, 1, 2, \dots$$

Let $\Psi_j^n = ((\psi_1)_j^n, \dots, (\psi_M)_j^n)^T$ be the approximation of $\Psi(x_j, t_n) = (\psi_1(x_j, t_n), \dots, \psi_M(x_j, t_n))^T$.

From time $t = t_n$ to $t = t_{n+1}$, the VGPEs (4.1) is solved in three splitting steps. One solves first

$$i \frac{\partial \Psi(x, t)}{\partial t} = -\frac{1}{2} \Psi_{xx}(x, t) \quad (4.4)$$

for the time step of length k , followed by solving

$$i \frac{\partial \Psi(x, t)}{\partial t} = \mathbf{V}_1(x) \dot{*} \Psi(x, t) + \mathbf{A}_1(\Psi(x, t)) \dot{*} \Psi(x, t), \quad (4.5)$$

for the same time step, and then by solving

$$i \frac{\partial \Psi(x, t)}{\partial t} = f(t) B \Psi(x, t), \quad (4.6)$$

Equations (4.4) will be discretized in space by the sine-spectral method and integrated in time *exactly*. For $t \in [t_n, t_{n+1}]$, the ODE system (4.5) leaves $|\psi_j(x, t)|$ ($j = 1, \dots, M$) invariant in t and therefore becomes

$$i \frac{\partial \Psi(x, t)}{\partial t} = \mathbf{V}_1(x) \dot{*} \Psi(x, t) + \mathbf{A}_1(\Psi(x, t_n)) \dot{*} \Psi(x, t), \quad (4.7)$$

and thus can be integrated *exactly*. The solution of (4.7) is

$$\Psi(x, t) = e^{-i(\mathbf{V}_1(x) + \mathbf{A}_1(\Psi(x, t_n)))(t-t_n)} \dot{*} \Psi(x, t_n), \quad t_n \leq t \leq t_{n+1}. \quad (4.8)$$

For $t \in [t_n, t_{n+1}]$, the ODE system (4.6) can be solve **exactly** too. In fact, since \hat{B} is real and symmetric, there exist an orthonormal real matrix P with $P^T = P^{-1}$ and a diagonal matrix $D = \text{diag}(d_1, \dots, d_M)$ such that

$$\hat{B} = P D P^T.$$

Thus the matrix B in (2.4) can be diagonalizable too, i.e.

$$B = G_0^{-1} P D P^T G_0. \quad (4.9)$$

Let

$$\Phi(x, t) = P^T G_0 \Psi(x, t), \quad (4.10)$$

Plugging (4.10) into (4.6), noting (4.9), we get

$$i \frac{\partial \Phi(x, t)}{\partial t} = f(t) D \Phi(x, t). \quad (4.11)$$

The solution of (4.11) is

$$\Phi(x, t) = e^{-i D \int_{t_n}^t f(s) ds} \Phi(x, t_n), \quad t_n \leq t \leq t_{n+1}. \quad (4.12)$$

Substituting (4.12) into (4.10), we obtain the solution of the ODE system (4.6)

$$\begin{aligned} \Psi(x, t) &= G_0^{-1} P e^{-i D \int_{t_n}^t f(s) ds} \Phi(x, t_n) \\ &= G_0^{-1} P e^{-i D \int_{t_n}^t f(s) ds} P^T G_0 \Psi(x, t_n), \quad t_n \leq t \leq t_{n+1}. \end{aligned} \quad (4.13)$$

From time $t = t_n$ to $t = t_{n+1}$, we combine the splitting steps via the standard second-order splitting:

$$\begin{aligned}
\Psi_j^{(1)} &= \frac{2}{N} \sum_{l=1}^{N-1} e^{-i k \mu_l^2/4} (\widehat{\Psi^n})_l \sin\left(\frac{i j l \pi}{N}\right), \\
\Psi_j^{(2)} &= e^{-i(\mathbf{V}_1(x_j) + \mathbf{A}_1(\Psi_j^{(1)}))k/2} * \Psi_j^{(1)}, \\
\Psi_j^{(3)} &= G_0^{-1} P e^{-iD \int_{t_n}^{t_{n+1}} f(s) ds} P^T G_0 \Psi_j^{(2)}, \\
\Psi_j^{(4)} &= e^{-i(\mathbf{V}_1(x_j) + \mathbf{A}_1(\Psi_j^{(3)}))k/2} * \Psi_j^{(3)}, \\
\Psi_j^{n+1} &= \frac{2}{N} \sum_{l=1}^{N-1} e^{-i k \mu_l^2/4} (\widehat{\Psi^{(4)}})_l \sin\left(\frac{i j l \pi}{N}\right), \quad 1 \leq j \leq N-1; \quad (4.14)
\end{aligned}$$

where $\widehat{\Psi}_l = ((\widehat{\psi_1})_l, \dots, (\widehat{\psi_M})_l)^T$ ($l = 1, \dots, N-1$), the sine coefficients of Ψ with $\Psi_0 = \Psi_N = \mathbf{0}$, are defined as

$$\mu_l = \frac{l\pi}{b-a}, \quad \widehat{\Psi}_l = \sum_{j=1}^{N-1} \Psi_j \sin\left(\frac{i j l \pi}{N}\right), \quad l = 1, \dots, N-1. \quad (4.15)$$

The overall time discretization error comes solely from the splitting, which is second order in k , and the spatial discretization is of spectral (i.e. ‘infinite’) order of accuracy. It is time reversible and time-transverse invariant if the VGPEs (2.4) is, i.e. $f \equiv 0$. Furthermore, for the stability of the TSSP (4.14), we have the following lemma, which shows that the total number of particles in the multi-component BEC is conserved for any given real-valued external driven field f , and the number of particles of each component is conserved when there is no external driven field, i.e. $f \equiv 0$.

Lemma 4.1 *The time-splitting sine-spectral (TSSP) method (4.14) is unconditionally stable and conserves the total number of particles in the multi-component BEC. In fact, for every mesh size $h > 0$ and time step $k > 0$,*

$$\begin{aligned}
\|G_0 \Psi^n\|_{l^2} &:= \sqrt{\sum_{l=1}^M N_l^0 \|\psi_l^n\|_{l^2}^2} = \sqrt{\sum_{l=1}^M N_l^0 h \sum_{j=1}^{N-1} |(\psi_l^n)_j|^2} \\
&= \|G_0 \Psi_0\|_{l^2} = \sqrt{\sum_{l=1}^M N_l^0} = \sqrt{N^0}, \quad n = 1, 2, \dots \quad (4.16)
\end{aligned}$$

Furthermore, when $f \equiv 0$ in (2.4), i.e. without external driven field, we have

$$\|(\psi_l^n)\|_{l^2} := \sqrt{h \sum_{j=1}^{N-1} |(\psi_l^n)_j|^2} = \|(\psi_l^0)\|_{l^2} = 1, \quad n = 1, \dots, \quad j = 1, \dots, M. \quad (4.17)$$

Proof: From (4.16), noting (4.14), Parsaval equality, we get

$$\begin{aligned} \|G_0 \Psi^{n+1}\|_{l^2}^2 &= \|G_0 \Psi^{(4)}\|_{l^2}^2 = \|G_0 \Psi^{(3)}\|_{l^2}^2 = \|P e^{-iD \int_{t_n}^{t_{n+1}} f(\cdot, s) ds} P^T G_0 \Psi^{(2)}\|_{l^2}^2 \\ &= \|G_0 \Psi^{(2)}\|_{l^2}^2 = \|G_0 \Psi^{(1)}\|_{l^2}^2 = \|G_0 \Psi^n\|_{l^2}^2, \quad n = 0, 1, \dots \end{aligned} \quad (4.18)$$

The conservation (4.16) is obtained from (4.18) by induction. When $f \equiv 0$, the proof of (4.17) follows the line of the analogous result for the linear Schrödinger equation by time-splitting Fourier-spectral approximation in [7, 5].

Remark 4.1 *When the definite integral $\int_{t_n}^{t_{n+1}} f(s) ds$ in (4.14) could not be evaluated analytically for some very complicated function f , it can be evaluated numerically using a numerical quadrature, e.g., the Simpson's rule*

$$\int_{t_n}^{t_{n+1}} f(s) ds \approx \frac{k}{4} [f(t_n) + 4f(t_n + k/2) + f(t_{n+1})], \quad j = 0, \dots, N, \quad n \geq 0.$$

Remark 4.2 *When $M = 2$, $b_{11} = b_{22} = 0$, $b_{12} = b_{21} = 1$ and $\hat{f}(t) = \Omega \cos(\omega_d t)$ in (2.1) [27], thus $f(t) = \frac{\Omega}{\omega_{x,1}} \cos(\omega_d t / \omega_{x,1})$ in (2.4). After a simple computation, we can get explicitly the solution (4.13) of the ODE system (4.6) which will be used in our numerical example 5 in the next section:*

$$\begin{aligned} \psi_1(x, t) &= \cos(g(t, t_n)) \psi_1(x, t_n) - i \sin(g(t, t_n)) \sqrt{N_2^0 / N_1^0} \psi_2(x, t_n), \\ \psi_2(x, t) &= -i \sin(g(t, t_n)) \sqrt{N_1^0 / N_2^0} \psi_1(x, t_n) + \cos(g(t, t_n)) \psi_2(x, t_n), \quad t_n \leq t \leq t_{n+1}; \end{aligned}$$

where

$$\begin{aligned} g(t, t_n) &= \int_{t_n}^t f(s) ds = \int_{t_n}^t \frac{\Omega}{\omega_{x,1}} \cos(\omega_d s / \omega_{x,1}) ds \\ &= \frac{\Omega}{\omega_d} [\sin(\omega_d t / \omega_{x,1}) - \sin(\omega_d t_n / \omega_{x,1})]. \end{aligned}$$

5 Numerical results

In this section we report the coupled basis wavefunctions with lowest energy of a two-state model and ground states of multi-component BEC by using the normalized gradient flow method, and dynamics of multi-component BEC by using the time-splitting sine-spectral method. Furthermore we also give a physical discussion on our numerical results.

Example 1 Coupled basis wavefunctions with lowest energy of a two-state model, i.e. we choose $\beta = 100$ and $F = 0.79$ in (3.37), (3.38). We solve this problem on $[0, 8]$, i.e. $R = 8$ with mesh size $h_r = \frac{1}{64}$ and time step $k = 0.1$ by using the BEFD discretization (3.46), (3.47). The initial data in (3.45) is chosen as

$$\phi_{s,0}(r) = \frac{1}{\pi^{1/2}} e^{-r^2/2}, \quad \phi_{v,0}(r) = \frac{r}{\pi^{1/2}} e^{-r^2/2}, \quad r \geq 0.$$

The steady state solution is reached when $\|\phi_s^{n+1} - \phi_s^n\|_{l^2} + \|\phi_v^{n+1} - \phi_s v^n\|_{l^2} < \varepsilon = 10^{-6}$. Table 1 displays the values of $\phi_s(0)$, energies E_s , E_v and E , chemical potentials μ_s , μ_v . Figure 1 shows the coupled basis wavefunctions $\phi_{s,g}(r)$ and $\phi_{v,g}(r)$ for different vortex fraction $0 \leq n_v \leq 1$, and Figure 2 shows surface plots of the atomic density function $|\psi|^2 = |a_s \phi_{s,g} + a_v \phi_{v,g} e^{i\theta}|^2$ with $a_v = \sqrt{n_v}$ and $a_s = \sqrt{1 - n_v}$ for different vortex fraction $0 \leq n_v \leq 1$.

n_v	n_s	$\phi_s(0)$	E_s	E_v	E	μ_s	μ_v
0	1	0.2381	3.9459	NA	3.9459	5.7598	NA
0.1	0.9	0.2517	3.8697	5.8901	4.0717	5.7939	6.9516
0.3	0.7	0.2875	3.7370	5.4928	4.2637	5.8864	6.6513
0.5	0.5	0.3433	3.6474	5.1110	4.3792	6.0166	6.4091
0.7	0.3	0.4450	3.6291	4.7618	4.4220	6.1946	6.2276
0.9	0.1	0.7113	3.7653	4.4637	4.3938	6.4023	6.0951
1	0	NA	NA	4.3689	4.3689	NA	6.0514

Table 1: Numerical results for a two-state model in 2d in Example 1.

From Table 1 and Figures 1&2, we can see that, when the vortex state fraction n_v increases from 0 to 1, the central value of the symmetric state $\phi_s(0)$ and the total energy E increase, chemical potentials of the symmetric state μ_s and vortex state μ_v increases and decreases, respectively; the atomic density function $|\psi|^2$ changes from ground state (cf. Fig. 2a) to vortex state (cf. Fig. 2f).

Example 2 Ground state of two-component BEC in 3d with dynamically stable inter-component interaction, i.e. $a_{11} > 0$, $a_{22} > 0$ and $a_{11}a_{22} - a_{12}^2 > 0$ [30]. We choose $M = 2$, $m = 1.44 \times 10^{-25}$ [kg], $a_{11} = a_{22} = 5.45$ [nm], $a_{12} = a_{21} = 5.24$ [nm], $\omega_{x,1} = \omega_{y,1} = \omega_{x,2} = \omega_{y,2} = 10 \times 2\pi$ [1/s], $\omega_{z,1} = \omega_{z,2} = \sqrt{8}\omega_{x,1}$, $\hat{x}_{0,1} = \hat{x}_{0,2} = \hat{y}_{0,1} = \hat{y}_{0,2} = \hat{z}_{0,1} = \hat{z}_{0,2} = 0$, $\hat{f} \equiv 0$ in (2.1). Plugging these parameters into (2.4), we get the dimensionless parameters $a_0 = 0.3407 \times 10^{-5}$ [m], $\beta_{11} = 0.02010177N_1^0$, $\beta_{12} = 0.0193272N_2^0$, $\beta_{21} = 0.0193272N_1^0$, $\beta_{22} = 0.02010177N_2^0$. We compute the ground states of this problem in cylindrical coordinate on $(r, z) \in \Omega = [0, 8] \times [-4, 4]$ with mesh size $h = h_r = h_z = \frac{1}{32}$ and time step $k = 0.1$ by using the BEFD discretization for different N_1^0 and N_2^0 . Here we report the results for two cases:

- Case I. $N_2^0 = N_1^0$;
Case II. $N_2^0 = 2N_1^0$.

Table 2 displays the central densities $\phi_{g,1}(0, 0)^2$, $\phi_{g,2}(0, 0)^2$, chemical potential $\mu_{g,1}$, $\mu_{g,2}$ and energy E_β for case I with different N_1^0 . Figure 3 shows the ground state condensate wave functions for case I. Furthermore Table 3 and Figure 4 show similar results for case II.

N_1^0	$\phi_{g,1}^2(0,0)$	$\mu_{g,1}$	$\phi_{g,2}^2(0,0)$	$\mu_{g,2}$	E
0	0.5496	2.4130	0.5496	2.4130	2.4130
100	0.4747	2.7664	0.4747	2.7664	2.5994
500	0.3548	3.6406	0.3548	3.6406	3.1161
1,000	0.2969	4.3481	0.2969	4.3481	3.5650
3,000	0.2170	6.0980	0.2170	6.0980	4.7258
6,000	0.1765	7.7461	0.1765	7.7461	5.8504
10,000	0.1513	9.3204	0.1513	9.3204	6.9388
20,000	0.1226	12.0802	0.1226	12.0802	8.8655

Table 2: Numerical results for the ground states of two-component BEC in 3d in example 2 for case I.

N_1^0	$\phi_{g,1}^2(0,0)$	$\mu_{g,1}$	$\phi_{g,2}^2(0,0)$	$\mu_{g,2}$	E
10	0.5353	2.4738	0.5351	2.4746	2.4440
100	0.4504	2.9062	0.4491	2.9122	2.6799
500	0.3225	4.0142	0.3193	4.0315	3.3582
1,000	0.2679	4.8777	0.2637	4.9029	3.9218
3,000	0.1963	6.9773	0.1902	7.0200	5.3429
6,000	0.1610	8.9353	0.1536	8.9931	6.6984
10,000	0.1392	10.7975	0.1309	10.8692	8.0013
20,000	0.1145	14.0520	0.1053	14.1471	10.2956

Table 3: Numerical results for the ground states of two-component BEC in 3d in example 2 for case II.

From Tables 2&3 and Figures 3&4, we can see that, when the number of particles of the two component are the same, i.e. $N_1^0 = N_2^0$, then the ground state density functions for the two components are equal to each other, i.e. $\phi_{g,1}^2 = \phi_{g,2}^2$ due to the same parameters used for the two components; where when $N_1^0 \neq N_2^0$, then $\phi_{g,1}^2 \neq \phi_{g,2}^2$. In the two cases, when the number of particles in the first condensate N_1^0 increases, the central value of the density functions $\phi_{g,1}^2(0,0)$ and $\phi_{g,2}^2(0,0)$ decrease, but the the total energy E , and the chemical potentials $\mu_{g,1}$ and $\mu_{g,2}$ increase.

Example 3 Ground state of two-component BEC in 3d with dynamically unstable inter-component interaction, i.e. $a_{11} > 0$, $a_{22} > 0$ and $a_{11}a_{22} - a_{12}^2 < 0$ [27]. We choose $M = 2$, $m = 1.44 \times 10^{-25}$ [kg], $a_{12} = a_{21} = 55.3\text{\AA} = 5.53$ [nm], $a_{11} = 1.03a_{12} = 5.6959$ [nm], $a_{22} = 0.97a_{12} = 5.3641$ [nm], $\omega_{z,1} = \omega_{z,2} = 47 \times 2\pi$ [1/s], $\omega_{x,1} = \omega_{y,1} = \omega_{x,2} = \omega_{y,2} = \omega_{z,1}/\sqrt{8}$, $\hat{x}_{0,1} = \hat{x}_{0,2} = \hat{y}_{0,1} = \hat{y}_{0,2} = 0$, $\hat{f} \equiv 0$ in (2.1). Plugging these parameters into (2.4), we get the dimensionless parameters $a_0 = 0.2643 \times 10^{-5}$ [m], $\beta_{11} = 0.02708165N_1^0$, $\beta_{12} = 0.02629286N_2^0$, $\beta_{21} = 0.02629286N_1^0$, $\beta_{22} = 0.02550407N_2^0$. We compute the ground states of this problem in cylindrical coordinate on $(r, z) \in \Omega = [0, 16] \times [-12, 12]$ with mesh size $h = h_r = h_z = \frac{1}{16}$ and time step $k = 0.1$ by using the BEFD discretization for different N_1^0 and N_2^0 . Here we report the results for three cases:

- Case I. $\hat{z}_{0,1} = \hat{z}_{0,2} = 0$, $N^0 = N_1^0 + N_2^0 = 1,000,000$. Varying the ratio between N_1^0 and N_2^0 ;
Case II. $N_2^0 = N_1^0 = 500,000$. $\hat{z}_{0,1} = -\hat{z}_{0,2} \neq 0$. Varying $\hat{z}_{0,1}$;
Case III. $\hat{z}_{0,1} = -\hat{z}_{0,2} = 0.15a_0$, $N^0 = N_1^0 + N_2^0 = 1,000,000$. Varying the ratio between N_1^0 and N_2^0 .

Table 4 displays the central densities $\phi_{g,1}(0,0)^2$, $\phi_{g,2}(0,0)^2$, chemical potential $\mu_{g,1}$, $\mu_{g,2}$ and energy E_β for case I with different N_1^0 . Figure 5 shows the ground state condensate wave functions for case I. Furthermore Table 5 and Figure 6 show similar results for case II and Table 6 and Figure 7 for case III.

N_1^0	N_2^0	$\phi_{g,1}^2(0,0)$	$\mu_{g,1}$	$\phi_{g,2}^2(0,0)$	$\mu_{g,2}$	E
100,000	900,000	0.0007	47.8143	0.0453	47.2278	33.8714
300,000	700,000	0.0025	47.9650	0.0514	47.2456	34.0028
500,000	500,000	0.0063	48.0880	0.0605	47.2631	34.1575
700,000	300,000	0.0129	48.1999	0.0759	47.2779	34.3323
900,000	100,000	0.0270	48.3077	0.1082	47.2873	34.5266

Table 4: Numerical results for the ground states of two-component BEC in 3d in example 3 for case I.

From Tables 4,5&6 and Figures 5,6&7, we can have the following observations:
(i). In case I, the trap potentials for the two components are the same, when the

$\hat{z}_{0,1}/a_0$	$\phi_{g,1}^2(0,0)$	$\mu_{g,1}$	$\phi_{g,2}^2(0,0)$	$\mu_{g,2}$	E
0.01	0.0092	48.0611	0.0601	47.2363	34.1375
0.1	0.0307	47.3400	0.0513	46.4531	33.5336
0.5	0.0370	43.9392	0.0425	43.0278	30.8042
2.0	0.0277	37.3581	0.0271	36.4870	26.2717
4.0	0.0001	36.7085	0.0000	35.8441	26.0203

Table 5: Numerical results for the ground states of two-component BEC in 3d in example 3 for case II.

N_1^0	N_2^0	$\phi_{g,1}^2(0,0)$	$\mu_{g,1}$	$\phi_{g,2}^2(0,0)$	$\mu_{g,2}$	E
100,000	900,000	0.0023	44.3215	0.0452	47.0379	33.4594
300,000	700,000	0.0129	45.9058	0.0502	46.5788	33.1356
500,000	500,000	0.0335	46.8865	0.0489	45.9868	33.1615
700,000	300,000	0.0463	47.6052	0.0285	45.1929	33.4916
900,000	100,000	0.0443	48.1503	0.0072	43.9508	34.1429

Table 6: Numerical results for the ground states of two-component BEC in 3d in example 3 for case III.

fraction of the number of particles in the first component, i.e. N_1^0/N^0 , increases, the energy E increases, and the chemical potentials for the two components, $\mu_{g,1}$ and $\mu_{g,2}$, increases and decreases, respectively. The reason of this is due to $a_{11} > a_{22}$. Furthermore, we observe a crater in the density function of the first component, corresponding to a shell in which the second component reside (cf. Fig. 5e&f). This confirms the experimental results (cf. Fig. 1 in [27]). (ii). In case II, when the distance between the center of the trap potentials for the two components, i.e. $\hat{z}_{0,1} - \hat{z}_{0,2}$, increases, the energy E , chemical potentials for the two components, $\mu_{g,1}$ and $\mu_{g,2}$, decrease. Furthermore, the bigger the distance, the more separation in the density functions of the two components (cf. Fig.6). (iii). The above observation (i) also holds for case III except that the crater in the density function for the first component almost disappears (cf. Fig. 7). This is due to the separation of the centers of the trap potentials for the two components.

Example 4 Dynamics of two-component BEC in 3d with dynamically unstable inter-component interaction, i.e. $a_{11} > 0$, $a_{22} > 0$ and $a_{11}a_{22} - a_{12}^2 < 0$ [27]. We choose $M = 2$, $m = 1.44 \times 10^{-25}$ [kg], $a_{12} = a_{21} = 55.3\text{\AA} = 5.53$ [nm], $a_{11} = 1.03a_{12} = 5.6959$ [nm], $a_{22} = 0.97a_{12} = 5.3641$ [nm], $\omega_{z,1} = \omega_{z,2} = 47 \times 2\pi$ [1/s], $\omega_{x,1} = \omega_{y,1} = \omega_{x,2} = \omega_{y,2} = \omega_{z,1}/\sqrt{8}$, $\hat{x}_{0,1} = \hat{x}_{0,2} = \hat{y}_{0,1} = \hat{y}_{0,2} = 0$, $\hat{z}_{0,1} = -\hat{z}_{0,2} = 0.15a_0$, $\hat{f}(\mathbf{x}, t) = \Omega \cos(\omega_d t)$ in (2.1). We start the simulation with the initial data chosen as the ground state of (2.4) computed by setting $f \equiv 0$ and using BEFD

discretization. We take $\omega_d = 6.5 \times 2\pi$ [1/s], $N_1^0 = N_2^0 = 500,000$, and solve this problem on the box $[-16, 16] \times [-16, 16] \times [-8, 8]$ with mesh sizes $h_x = h_y = 1/4$, $h_z = 1/8$ and time step $k = 0.0002$. Figure 8 shows the time evolution of the mean of the density functions for the two components, $\|\psi_1\|^2$, $\|\psi_2\|^2$ (noticing that the number of particles in the two components are $N_1^0\|\psi_1\|^2$, $N_2^0\|\psi_2\|^2$, respectively) for $\Omega = 6.5 \times 2\pi$ [1/s], $65 \times 2\pi$ [1/s] and $650 \times 2\pi$ [1/s]. Furthermore Figure 9 displays the time evolution of the density functions for the two components for $\Omega = 65 \times 2\pi$ [1/s].

The general form of time evolution on the number of particles in the two components is similar for different external driven field frequency Ω . When Ω is small, the number of particles in the first component, i.e. $N_1^0\|\psi_1\|^2$, increases, attains its peak and then decreases; where the pattern for $N_2^0\|\psi_2\|^2$ is opposite (cf. Fig. 8a), which is due to the total number of particles in the two components are conserved. When Ω becomes bigger, the pattern of $N_1^0\|\psi_1\|^2$ oscillates for some time period, attains its absolute peak, and then oscillates again (cf. Fig. 8b). Initially the density functions for the two components are well separated (cf. Fig. 9 first row), around at time $t = 3.4$, the number of particles in the first component attains its maximum and a bigger condensate (with approximately 52% bigger in term of the number of particles for the first component than that initially at time $t = 0$) is generated (cf. Fig. 8b&9). When Ω becomes very big, similar pattern of $N_1^0\|\psi_1\|^2$ is observed. In fact, the bigger Ω is, the faster oscillation in the pattern of the number of particles in the condensates (cf. Fig. 8a,b&c).

6 Conclusions

The ground states and dynamics of multi-component Bose-Einstein condensates at temperature T much smaller than the critical condensate temperature T_c are studied numerically by using the time-independent vector Gross-Pitaevskii equations (VGPRs) and time-dependent VGPEs with (or without) an external driven field, respectively. We started with the 3d VGPEs, scale it to obtain a dimensionless VGPEs, and showed how to approximately reduce it to a 2d VGPEs and a 1d VGPEs in certain limits. We provided the approximate ground state solution of the VGPEs in the (very) weakly interacting condensates. Then, most importantly, we presented a normalized gradient flow (NGF) to compute ground states of multi-component BEC, proved energy diminishing of the NGF which provides a mathematical justification, discretized it by the backward Euler finite difference (BEFD) which is monotone in linear and nonlinear cases and preserves energy diminishing property in linear case; as well as we used a time-splitting sine-spectral method (TSSP) to discretize the time-dependent VGPEs with an external driven field for computing dynamics of multi-component BEC. The merit of the TSSP for VGPEs is that it is explicit, unconditionally stable, easy to program, less memory requirement, time reversible and time transverse invariant if the VGPEs is, ‘good’ resolution in the

semiclassical regime, of spectral order accuracy in space and second order accuracy in time, and conserves the total particle number in the discretized level. Extensive numerical examples in 3d for ground states and dynamics of multi-component BEC are presented to demonstrate the power of the numerical methods. Finally, we want to point out that equations very similar to the VGPEs are also encountered in non-linear optics. In the future we plan to apply the powerful numerical methods to study vortex states and their dynamical stability in multi-component Bose-Einstein condensates.

Acknowledgment

The author acknowledges support by the National University of Singapore grant No. R-151-000-027-112 and helpful discussions with D. Jaksch and P. Markowich. This work was also supported in part by the WITTGENSTEIN-AWARD of P. Markowich which is funded by the Austrian National Science Foundation FWF.

References

- [1] A. Aftalion A, and Q. Du, Vortices in a rotating Bose-Einstein condensate: Critical angular velocities and energy diagrams in the Thomas-Fermi regime, *Phys. Rev. A*, 64(2001), pp. 063603.
- [2] M.H. Anderson, J.R. Ensher, M.R. Matthews, C.E. Wieman, and E.A. Cornell, Observation of Bose-Einstein condensation in a dilute atomic vapor, *Science*, 269(1995), pp. 198-201.
- [3] J.R. Anglin and W. Ketterle, Bose-Einstein condensation of atomic gases, *Nature*, 416(2002), pp. 211-218.
- [4] W. Bao and Q. Du, Computing the ground state solution of Bose-Einstein condensates by a normalized gradient flow, preprint.
- [5] W. Bao, D. Jaksch, An explicit unconditionally stable numerical methods for solving damped nonlinear Schrodinger equations with a focusing nonlinearity, *SIAM J. Numer. Anal.*, to appear.
- [6] W. Bao, D. Jaksch and P.A. Markowich, Numerical solution of the Gross-Pitaevskii equation for Bose-Einstein condensation, *J. Comput. Phys.*, 187(2003), pp. 318 - 342.
- [7] W. Bao, S. Jin and P.A. Markowich, On time-splitting spectral approximations for the Schrödinger equation in the semiclassical regime, *J. Comput. Phys.*, 175(2002), pp. 487-524.

- [8] W. Bao, S. Jin and P.A. Markowich, Numerical study of time-splitting spectral discretizations of nonlinear Schrödinger equations in the semi-classical regimes, *SIAM J. Sci. Comp.*, to appear.
- [9] W. Bao and F.F Sun, Numerical Simulation of the Vector Zakharov System for Multi-component Plasma, preprint.
- [10] W. Bao, F.F Sun and G.W. Wei, Numerical methods for the generalized Zakharov system, *J. Comput. Phys.*, in press.
- [11] W. Bao and W. Tang, Ground state solution of trapped interacting Bose-Einstein condensate by directly minimizing the energy functional, *J. Comput. Phys.*, 187(2003), pp. 230 - 254.
- [12] C.C. Bradley, C.A. Sackett, R.G. Hulet, *Phys. Rev. Lett.* 78, 985, 1997.
- [13] K.B. Davis, M.O. Mewes, M.R. Andrews, N.J. van Druten, D.S. Durfee, D.M. Kurn, and W. Ketterle, *Phys. Rev. Lett* **75**, 3969 (1995).
- [14] B.M. Caradoc-Davis, R.J. Ballagh and K. Burnett, Coherent dynamics of vortex formation in trapped Bose-Einstein condensates, *Phys. Rev. Lett.*, 83(1999), pp. 895.
- [15] B.M. Caradoc-Davis, R.J. Ballagh and P.B. Blakie, Three-dimensional vortex dynamics in Bose-Einstein condensates, *Phys. Rev. A*, 62(2000), pp. 011602.
- [16] M.M. Cerimele, M.L. Chiofalo, F. Pistella, S. Succi and M.P. Tosi, Numerical solution of the Gross-Pitaevskii equation using an explicit finite-difference scheme: An application to trapped Bose-Einstein condensates, *Phys. Rev. E*, 62(2000), pp. 1382-1389.
- [17] M.M. Cerimele, F. Pistella and S. succi, Particle-inspired scheme for the Gross-Pitaevski equation: An application to Bose-Einstein condensation, *Comput. Phys. Comm.*, 129(2000), pp. 82-90.
- [18] G.-H. Chen and Y.-S. Wu, Quantum phase transition in a multi-component Bose-Einstein condensate in optical lattices, *cond-mat/0205440*, 2002.
- [19] M.L. Chiofalo, S. Succi and M.P. Tosi, Ground state of trapped interacting Bose-Einstein condensates by an explicit imaginary-time algorithm, *Phys. Rev. E*, 62(2000), pp. 7438-7444.
- [20] Ph. W. Courteille, V.S. Bagnato and Y.I. Yukalov, Bose-Einstein condensation of trapped atomic gases, *cond-mat/0109421*, 2001.
- [21] R.J. Dodd, Approximate solutions of the nonlinear Schrödinger equation for ground and excited states of Bose-Einstein condensates, *J. Res. Natl. Inst. Stan.*, 101(1996), pp. 545-552.

- [22] M. Edwards and K. Burnett, Numerical solution of the nonlinear Schrödinger equation for small samples of trapped neutral atoms, *Phys. Rev. A*, 51(1995), pp. 1382-1386.
- [23] B.D. Esry, C.H. Greene, J.P. Burke, Jr. and J.L. Bohn, *Phys. Rev. Lett.*, 78 (1997), pp. 3594.
- [24] E.V. Goldstein, M.G. Moore, H. Pu and P. Meystre, Eliminating the mean-field shift in multicomponent Bose-Einstein condensates, *cond-mat/0005025*, 2000.
- [25] P. Ghosh, Exact results on the dynamics of multi-component Bose-Einstein condensate, *cond-mat/0111523*, 2002.
- [26] E.P. Gross, *Nuovo. Cimento.*, 20(1961), pp. 454.
- [27] D.S. Hall, M.R. Matthews, J.R. Ensher, C.E. Wieman and E.A. Cornell, Dynamics of component separation in a binary mixture of Bose-Einstein condensates, *Phys. Rev. Lett.*, 81 (1998), pp. 1539-1542.
- [28] T.-L. Ho and V.B. Shenoy, *Phys. Rev. Lett.*, 77 (1996), pp. 3276.
- [29] D. Jaksch, C. Bruder, J. I. Cirac, C. W. Gardiner, and P. Zoller, Cold bosonic atoms in optical lattices, *Phys. Rev. Lett.*, 81(1998), pp. 3108-3111.
- [30] D. Jaksch, S. A. Gardiner, K. Schulze, J. I. Cirac, and P. Zoller, Uniting Bose-Einstein condensates in optical resonators, *Phys. Rev. Lett.*, 86(2001), pp. 4733-4736.
- [31] T. Isoshima, K. Machida and T. Ohmi, Quantum vortex in a vectorial Bose-Einstein condensate, *cond-mat/0011421*, 2001.
- [32] I.M. Khalatnikov, *Zh. Eksp. Teor. Fiz.*, 32 (1957), pp. 653.
- [33] T. Kita, T. Mizushima and K. Machida, Spinor Bose-Einstein condensates with many vortices, *cond-mat/0204025*, 2002.
- [34] L. Landau and E. Lifschitz, *Quantum Mechanics: non-relativistic theory*, Pergamon Press, New York, 1977.
- [35] C.K. Law, H. Pu, N.P. Bigelow and J.H. Eberly, *Phys. Rev. Lett.*, 79 (1997), pp. 3594.
- [36] A.E. Leanhardt, Y. Shin, D. Kielpinski, D.E. Pritchard and W. Ketterle, Coreless vortex formation in a spinor Bose-Einstein condensate, *cond-mat/0212539*, 2002.
- [37] I. N. Levine, *Quantum Chemistry (Fifth Edition)* (Prentice Hall International, Inc., New York, 1991).

- [38] E.H. Lieb, R. Seiringer and J. Yngvason, Bosons in a Trap: A Rigorous Derivation of the Gross-Pitaevskii Energy Functional, *Phys. Rev. A*, 61(2000), pp. 3602.
- [39] C.J. Myatt et al., *Phys. Rev. Lett.*, 78(1997), pp. 985.
- [40] L.P. Pitaevskii, *Zh. Eksp. Teor. Fiz.*, 40(1961), pp. 646. (*Sov. Phys. JETP*, 13(1961), pp. 451).
- [41] H. Pu and N.P. Bigelow, *Phys. Rev. Lett.*, 80 (1998), pp. 1130.
- [42] P.A. Ruprecht, M.J. Holland, K. Burrett and M. Edwards, Time-dependent solution of the nonlinear Schrödinger equation for Bose-condensed trapped neutral atoms, *Phys. Rev. A*, 51(1995), pp. 4704-4711.
- [43] B.I. Schneider and D.L. Feder, Numerical approach to the ground and excited states of a Bose-Einstein condensated gas confined in a completely anisotropic trap, *Phys. Rev. A*, 59(1999), pp. 22332-2242.
- [44] E.D. Siggia and A.E. Ruckenstein, *Phys. Rev. Lett.*, 44 (1980), pp. 1423.
- [45] D.M. Stamper-Kurn et al. *Phys. Rev. Lett.*, 80 (1998), pp. 2027.
- [46] L. Simon, Asymptotics for a class of nonlinear evolution equations, with applications to geometric problems, *Annals of Math.*, 118(1983), pp. 525-571.

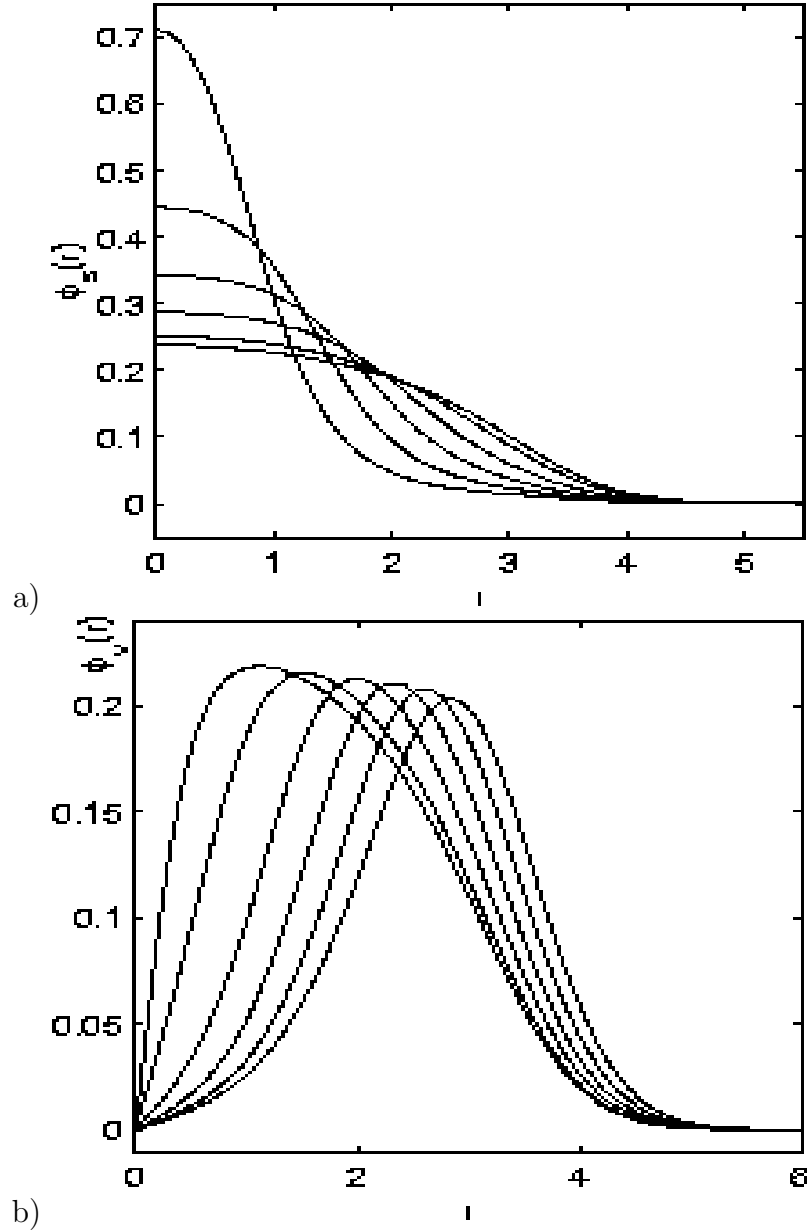


Figure 1: The coupled basis wavefunctions for a two-state model in example 1 for different vortex fraction $n_v = 0, 0.1, 0.3, 0.5, 0.7, 0.9, 1$ (in the order of decreasing peak). a). Symmetric state $\phi_{s,g}(r)$, b). Vortex state $\phi_{v,g}(r)$.

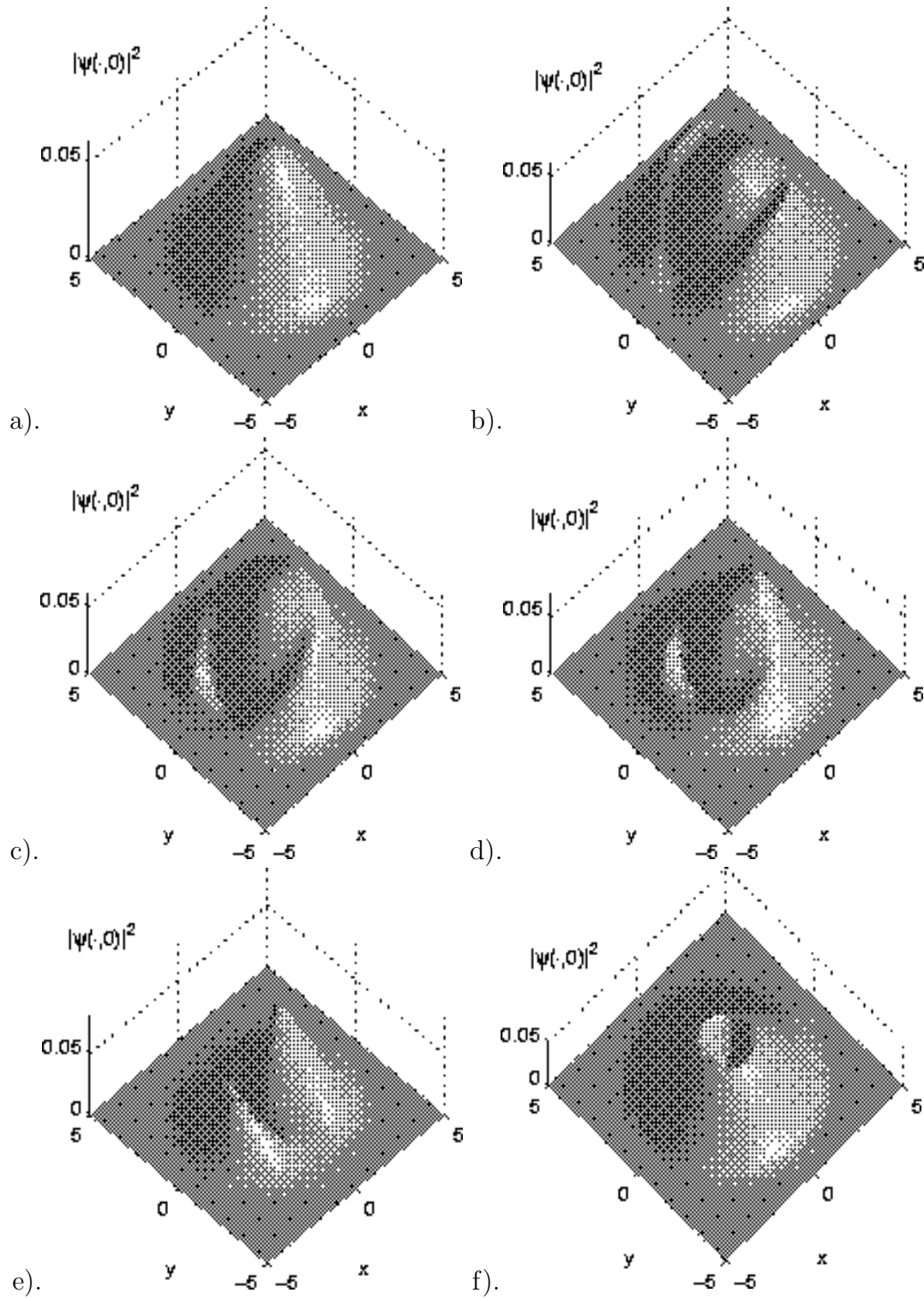


Figure 2: Surface plot of the atomic density function $|\psi|^2$ for different vortex fraction $0 \leq n_v \leq 1$. a). $n_v = 0$, b). $n_v = 0.1$, c). $n_v = 0.3$, d). $n_v = 0.5$, e). $n_v = 0.9$, f). $n_v = 1.0$.

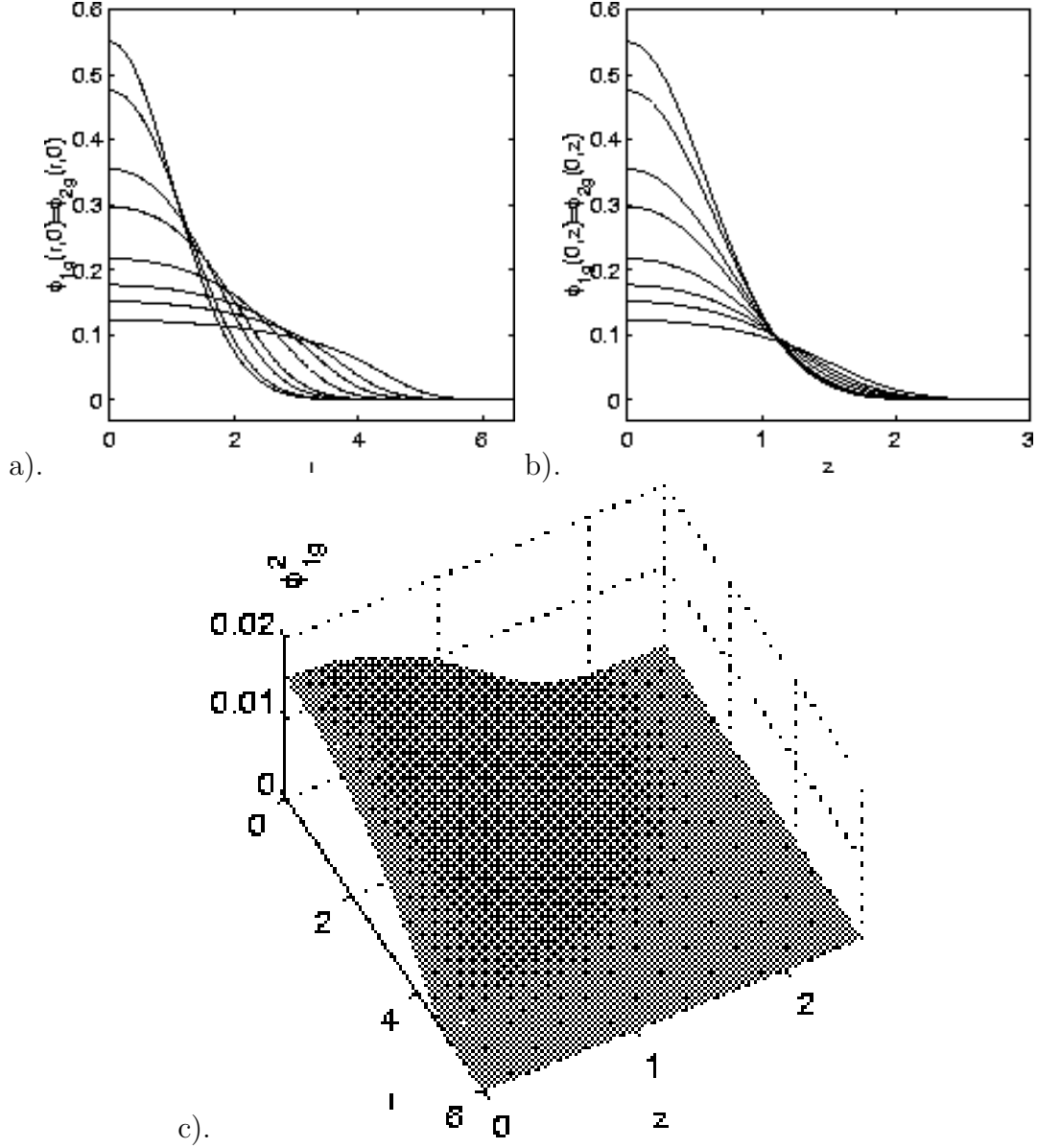


Figure 3: Ground state solution in 3d with cylindrical symmetry in example 2 for case I. Condensate wave function on two lines for $N_1^0 = 0, 100, 500, 1000, 3000, 6000, 10000, 20000$ (in the order of decreasing peak): a). On the line $z = 0$ $\phi_{g,1}(r, 0) = \phi_{g,2}(r, 0)$; b). On the line $r = 0$ $\phi_{g,1}(0, z) = \phi_{g,2}(0, z)$. c). Surface plot of the condensate density function $|\phi_{g,1}|^2 = |\phi_{g,2}|^2$ for $N_1^0 = 20000$.

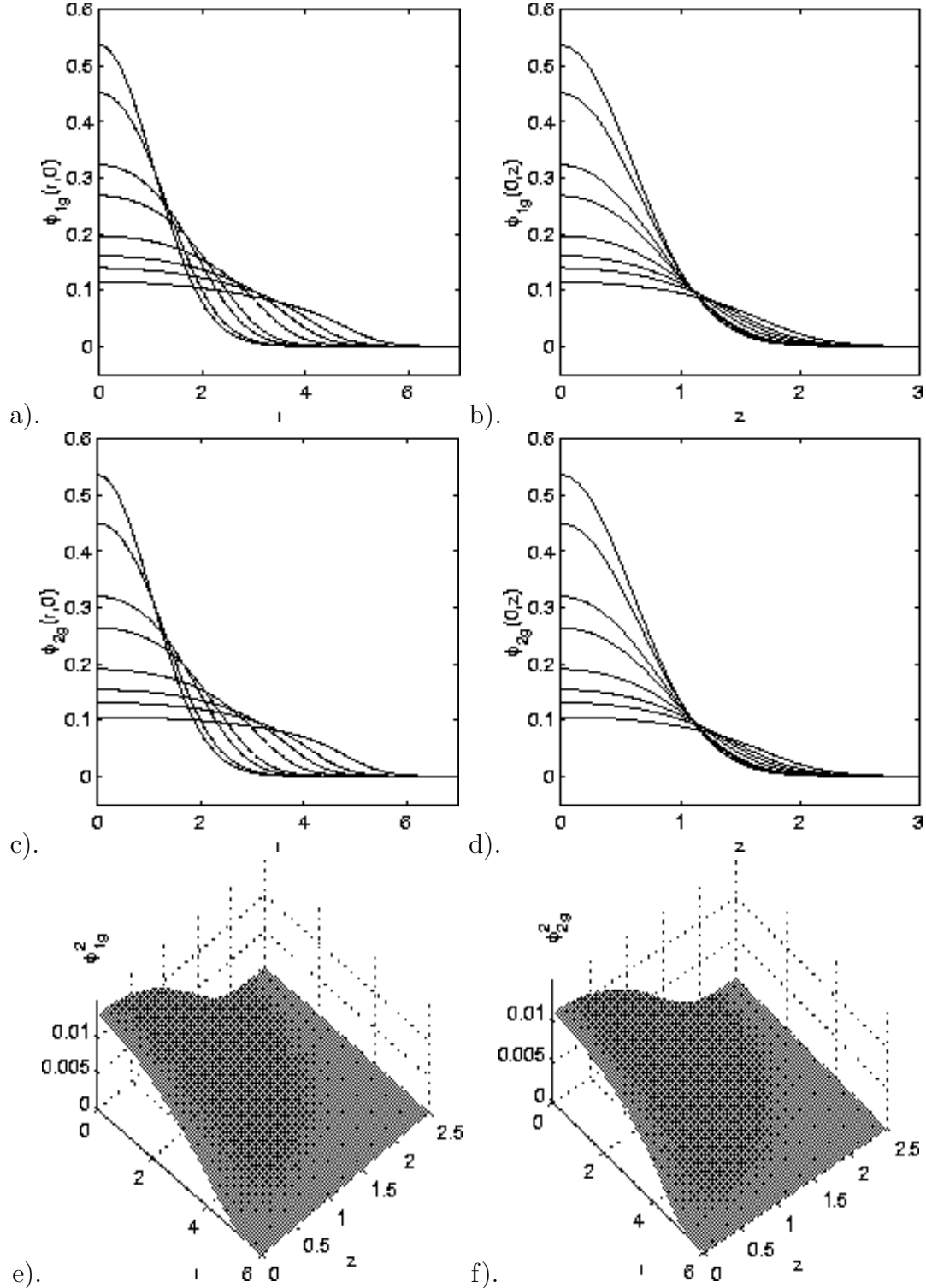


Figure 4: Ground state solution in 3d with cylindrical symmetry in example 2 for case II. Condensate wave function on two lines for $N_1^0 = 10, 100, 500, 1000, 3000, 6000, 10000, 20000$ (in the order of decreasing peak). On the line $z = 0$: a). $\phi_{g,1}(r, 0)$; c). $\phi_{g,2}(r, 0)$. On the line $r = 0$: b). $\phi_{g,1}(0, z)$; d). $\phi_{g,2}(0, z)$. Surface plot of the condensate density functions for $N_1^0 = 20000$: e). $|\phi_{g,1}|^2$; f). $|\phi_{g,2}|^2$.

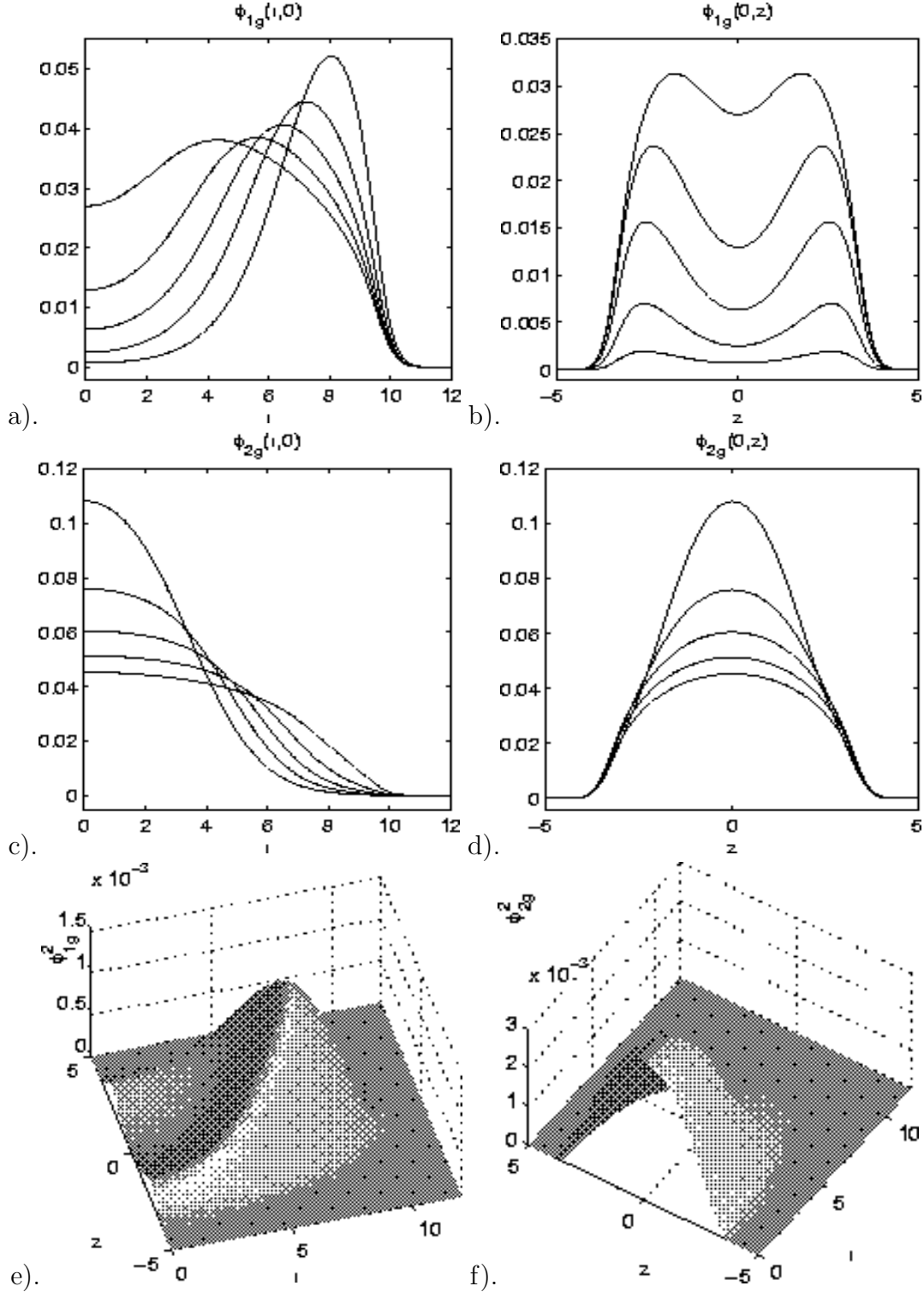


Figure 5: Ground state solution in 3d with cylindrical symmetry in example 3 for case I. Condensate wave function on two lines for $N_1^0/N^0 = 0.1, 0.3, 0.5, 0.7, 0.9$ (in the order of increasing at the origin). On the line $z = 0$: a). $\phi_{g,1}(r, 0)$; c). $\phi_{g,2}(r, 0)$. On the line $r = 0$: b). $\phi_{g,1}(0, z)$; d). $\phi_{g,2}(0, z)$. Surface plot of the condensate density functions for $N_1^0 = N_2^0 = 500,000$: e). $|\phi_{g,1}|^2$; f). $|\phi_{g,2}|^2$.

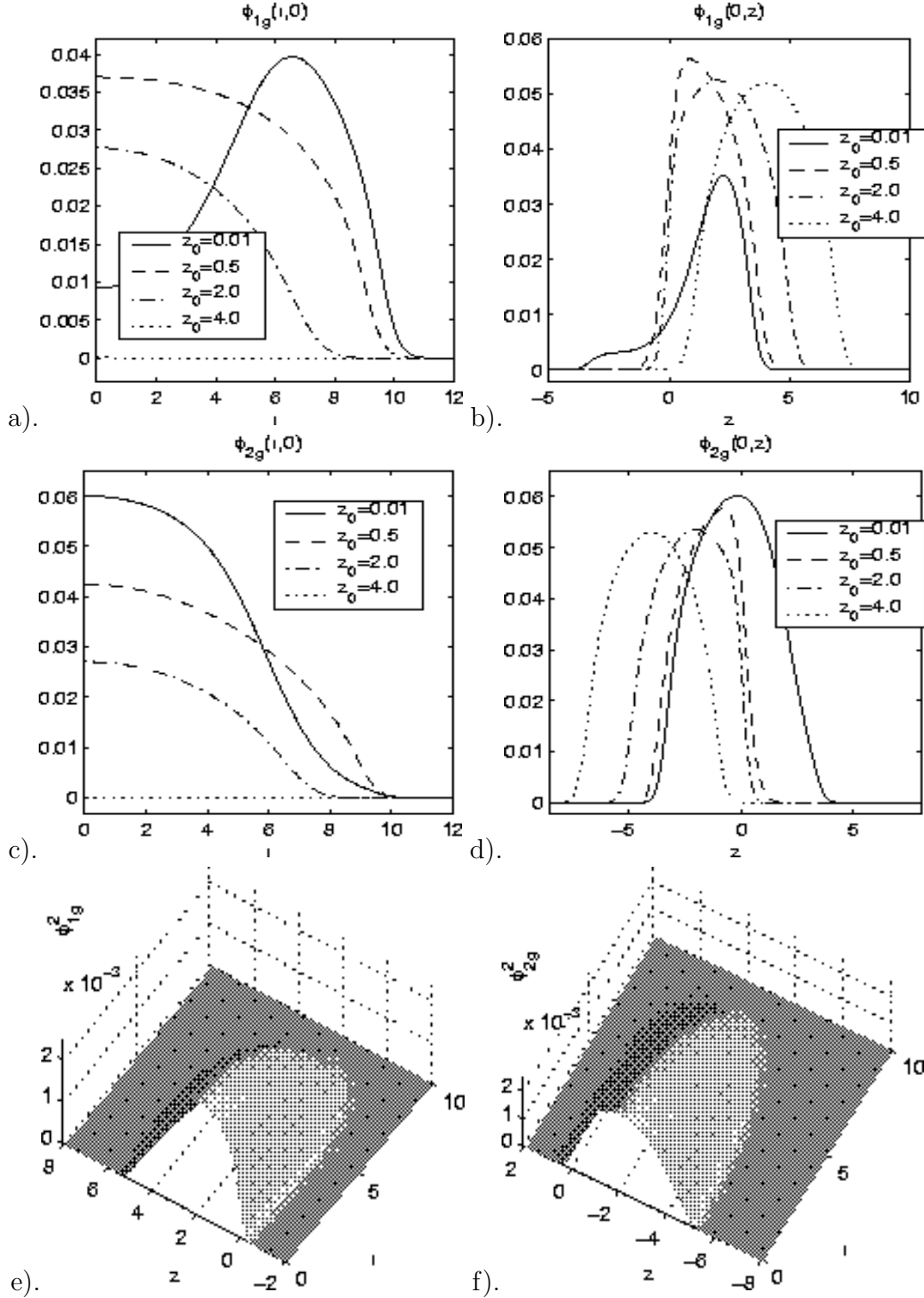


Figure 6: Ground state solution in 3d with cylindrical symmetry in example 3 for case II. Condensate wave function on two lines for $\hat{z}_{0,1}/a_0 = -\hat{z}_{0,2}/a_0 = 0.01, 0.1, 0.5, 2.0, 4.0$. On the line $z = 0$: a). $\phi_{g,1}(r, 0)$; c). $\phi_{g,2}(r, 0)$. On the line $r = 0$: b). $\phi_{g,1}(0, z)$; d). $\phi_{g,2}(0, z)$. Surface plot of the condensate density functions for $\hat{z}_{0,1}/a_0 = -\hat{z}_{0,2}/a_0 = 2.0$: e). $|\phi_{g,1}|^2$; f). $|\phi_{g,2}|^2$.

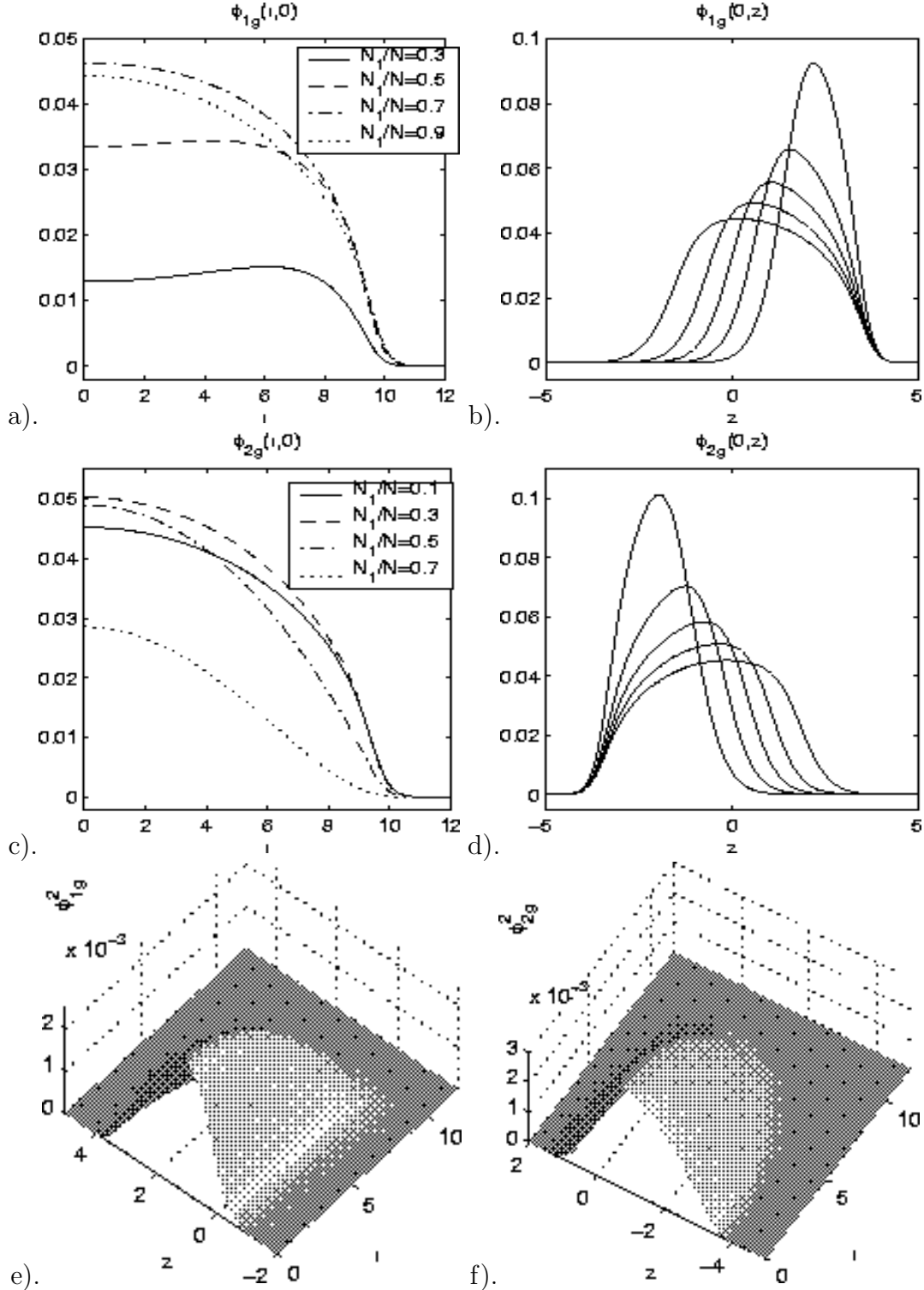


Figure 7: Ground state solution in 3d with cylindrical symmetry in example 3 for case III. Condensate wave function on two lines for $N_1^0/N^0 = 0.1, 0.3, 0.5, 0.7, 0.9$. On the line $z = 0$: a). $\phi_{g,1}(r, 0)$; c). $\phi_{g,2}(r, 0)$. On the line $r = 0$: b). $\phi_{g,1}(0, z)$ (in the order of decreasing peak); d). $\phi_{g,2}(0, z)$ (in the order of increasing peak). Surface plot of the condensate density functions for $N_1^0 = N_2^0 = 500,000$: e). $|\phi_{g,1}|^2$; f). $|\phi_{g,2}|^2$.

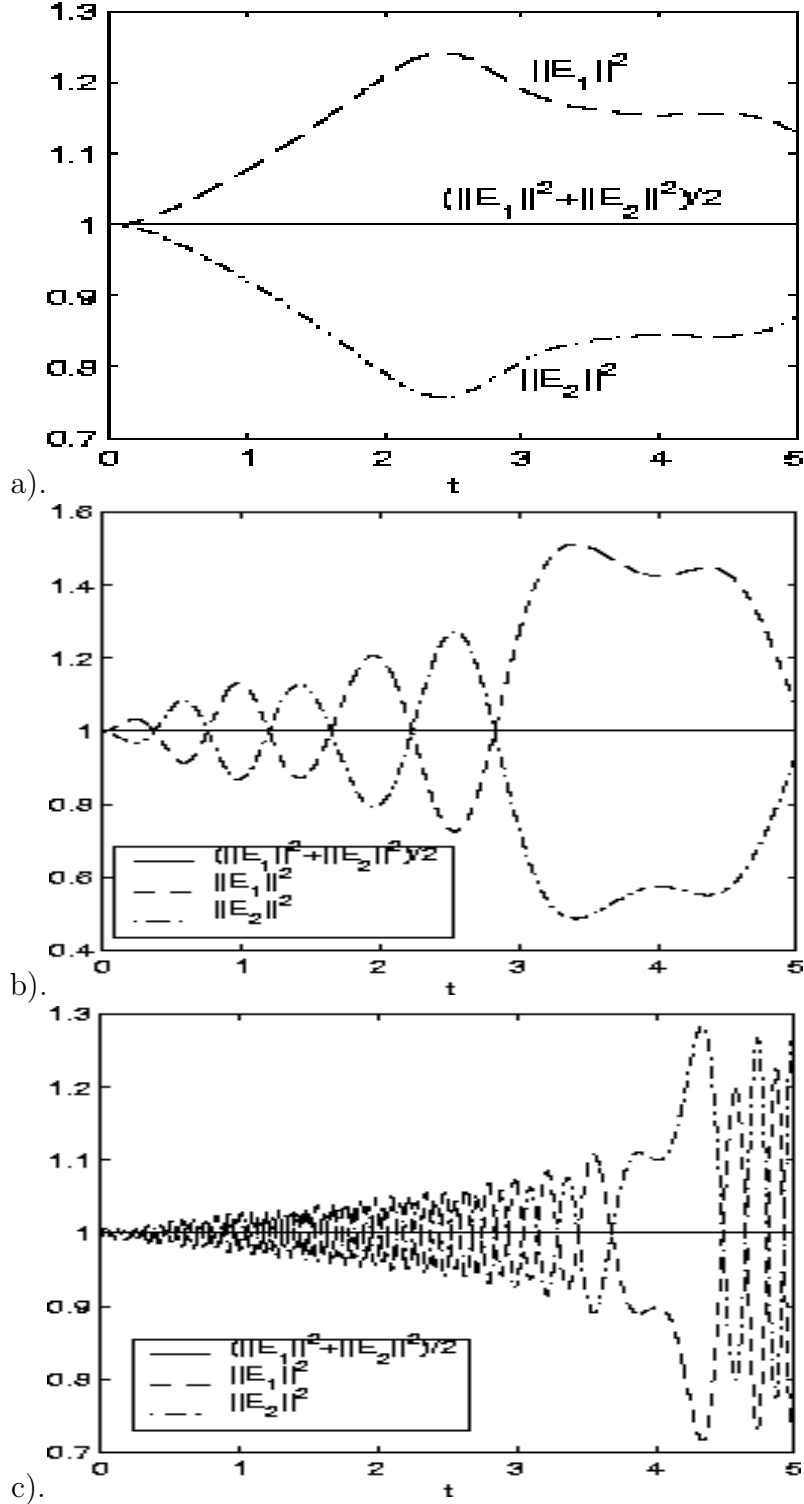


Figure 8: Time evolution of the mean of the density functions for the two components, $\|\psi_1\|^2$, $\|\psi_2\|^2$ (labeled as $\|E_1\|^2$ and $\|E_2\|^2$, respectively, which indicates the time evolution of the number of particles in the two components, $N_1^0\|\psi_1\|^2$, $N_2^0\|\psi_2\|^2$, respectively) for different driven field frequencies Ω . a). $\Omega = 6.5 \times 2\pi$ [1/s]; b). $65 \times 2\pi$ [1/s]; c). $650 \times 2\pi$ [1/s].

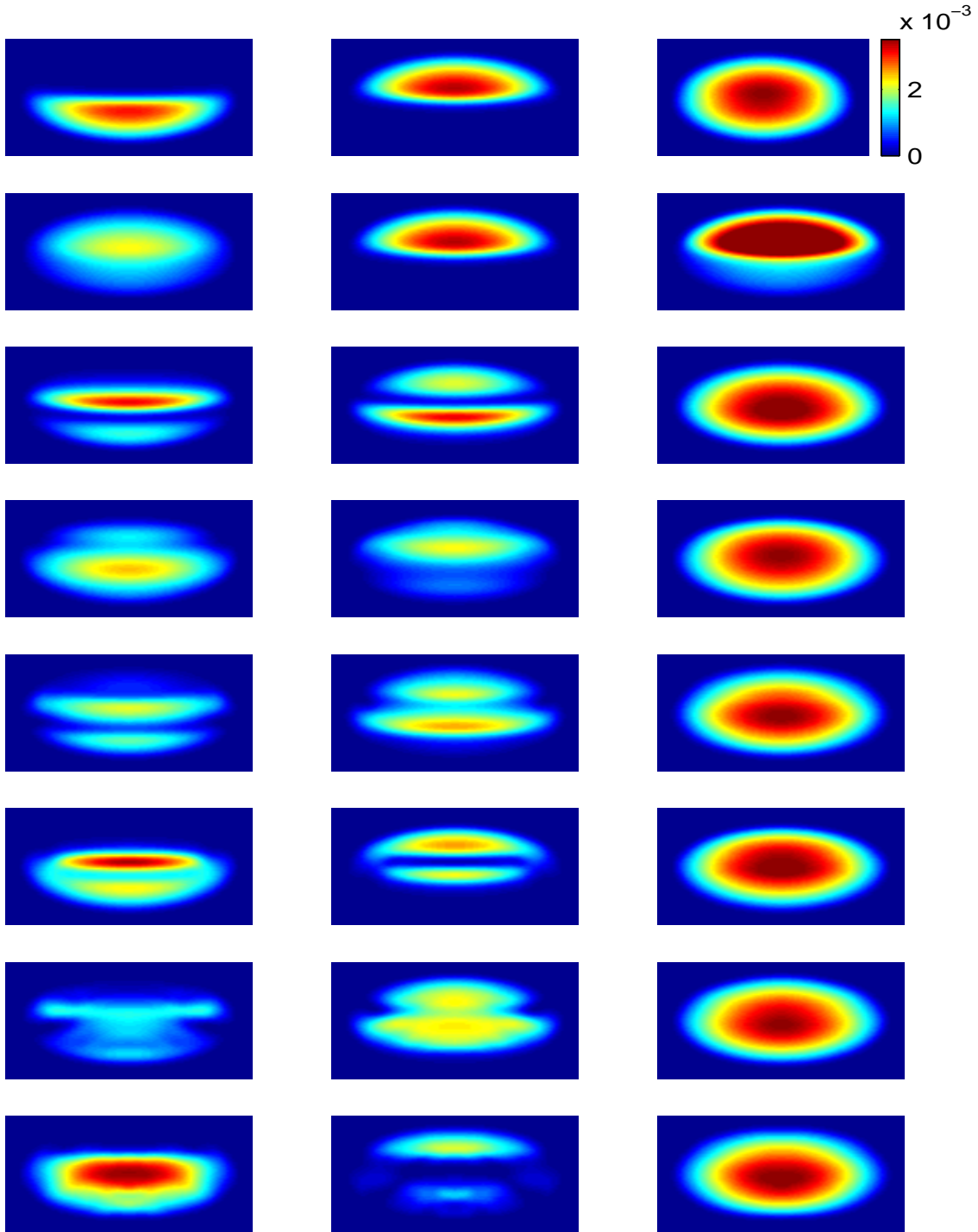


Figure 9: Time evolution of the density functions for the two components for the driven field frequencies $\Omega = 65 \times 2\pi$ [1/s] at different time, from top to bottom: $t = 0.0, 0.24, 0.58, 0.98, 1.42, 1.96, 2.52, 3.4$. Left column: $|\psi_1|^2$; middle column: $|\psi_2|^2$, right column: $|\psi_1|^2 + |\psi_2|^2$.

